From oblique accretion to transpression in the evolution of the Altaid collage: New insights from West Junggar, northwestern China

Flavien Choulet, Michel Faure, Dominique Cluzel, Yan Chen, Wei Lin, Bo Wang

From oblique accretion to transpression in the evolution of the Altaid collage: new insights from West Junggar, northwestern China

Flavien Choulet[1,*], Michel Faure[1], Dominique Cluzel[2], Yan Chen[1], Wei Lin[3], Bo Wang[4]

[1]: Institut des sciences de la Terre d'Orléans, UMR 6113 - CNRS/Université d'Orléans 1A, rue de la Férollerie, 45071 Orléans CEDEX 2, France

[2]: Pôle Pluridisciplinaire de la Matière et de l'Environnement, EA 3325, Université de la Nouvelle-Calédonie, Nouméa, Nouvelle-Calédonie, France

[3]: State Key Laboratory of Lithospheric Evolution, Institute of Geology and Geophysics, Chinese Academy of Sciences, P.O. Box 9825, Beijing 100029, China.

[4] : Department of Earth Sciences, Nanjing University, Nanjing, China

*: flavien.choulet@univ-orleans.fr

Abstract

Along active margins, tectonic features that develop in response to plate convergence are strongly controlled by subduction zone geometry. In West Junggar, a segment of the giant Palaeozoic collage of Central Asia, the West Karamay Unit represents a Carboniferous accretionary complex composed of fore-arc sedimentary rocks and ophiolitic mélanges. The occurrence of quasi-synchronous upright folds and folds with vertical axes suggests that transpression plays a significant role in the tectonic evolution of the West Junggar. Latest Carboniferous (ca. 300 Ma) alkaline plutons postdate this early phase of folding, which was synchronous with accretion of the Carboniferous complex. The Permian Dalabute sinistral fault overprints Carboniferous ductile shearing and split the West Karamay Unit ca. 100

kilometres apart. Oblique convergence may have been provoked by the buckling of the Kazakh orocline and relative rotations between its segments. Depending upon the shape of the convergence zone, either upright folds and fold with vertical axes, or alternatively, strike-slip brittle faults developed in response to strain partitioning. Sinistral brittle faulting may account for the lateral imbrication of units in the West Junggar accretionary complex.

Keywords

Altaids, West Junggar, oblique convergence, Late Paleozoic, transpression

1. Introduction

In contrast with strictly frontal convergence, which is rarely observed, examples of oblique subduction are widespread (Chamot-Rooke and Rabaute, 2007), and often generate strike-slip faults parallel to the upper plate boundary (Allen, 1965; Katili, 1970). The western North American Cordilleras, Andes, Taiwan, and Sumatra are the best examples of such an oblique convergent setting. Fitch (1972) was the first to link the tectonic structures in the upper plate to the oblique slip of the lower plate. Based on earthquake focal mechanisms in western Pacific, he proposed that the total decoupling of the oblique slip would result into a component of convergence normal to the trench and a shearing component parallel to the trench marked by transcurrent faulting. Beck (1983) improved this model by establishing the geometric and thermal constraints that favour decoupling of oblique convergence. Very oblique convergence, gently dipping subduction and thermal softening of the upper plate are the main conditions that favour the decoupling of oblique slip in a subduction zone.

Because total decoupling of oblique convergence is rarely achieved at sites of oceanic subduction, McCaffrey (1992) proposed a partial decoupling model, and demonstrated that margin geometry could influence the tectonic response of the upper plate. Therefore, oblique convergence along a concave or a convex subduction zone toward the ocean will be

accommodated by transpression or transtension, respectively. The present curvature of the western Sunda and Aleoutian subduction zones (Ekström and Engdahl, 1989; McCaffrey, 1991) are good paradigms of oblique slip partitioning that may also be reproduced by analogical modelling (Chemenda et al., 2000). The rheology of the accretionary wedge also influences the geometric variability of the subduction zone (Platt, 1993). Very oblique convergence would logically generate an intense slicing of the upper plate boundary (Martinez et al., 2002). Triple junctions and ridge subduction can also account for the initiation or reactivation of strike-slip faults in the overriding plate (Thorkelson, 1996; Roeske et al., 2003).

Lateral tectonic transport along the active margin is a direct consequence of decoupling (Coney et al., 1980; Beck, 1983; Jarrard, 1986); it is referred as "Sunda style" tectonics (Beck, 1983), and thousands of kilometres along-margin displacements have been evidenced in far-travelled allochthonous terranes of western North America (Beck, 1980; Coney et al., 1980). However, in most cases, terrane traveling is limited to a few tens of kilometres (Beck, 1986). This variability depends upon the age and obliquity of the subduction, and occurrence of a buttress or not (Beck, 1991). Therefore, oblique convergence that may result in lateral terrane transport significantly contributes to lateral growth of the continental margin and, consequently, to a reorganisation of the continental crust pattern.

During the last decades, Mesozoic and Cenozoic cases of oblique subduction have been established in the Circum-Pacific area, (Karig et al., 1978; Engebretson et al., 1985; Kimura, 1986; Reutter et al., 1991; Beck, 1994; Kusky et al., 1997a, b) by comparison with modern analogues (Malod et al., 1995; Lallemand et al., 1999; Goldfinger et al., 1996). In contrast, oblique subduction is rarely documented in older accretionary orogens (Henderson, 1987; Veevers, 2003). The purpose of this article is to report an example of Palaeozoic oblique convergence and to discuss its regional geodynamic controls.

The Altaids (Sengör et al., 1993; Sengör and Natal'in, 1996) or Central Asian Orogenic Belt (CAOB; Mossakovsky et al., 1993; Windley et al., 2007) are a wide orogenic collage formed during the Palaeozoic as a result of the convergence of Siberia, Baltica, Tarim, and North China blocks (Fig. 1a). Because of post-Palaeozoic tectonics, the present structure exhibits a distorted pattern of accretionary complexes, magmatic arcs, and ribbon-like micro continents. Several conflicting models have been proposed for the Altaids (for a review see Windley et al., 2007 and Xiao et al., 2010). The Kipchak Arc model is characterized by a single long-lived subduction that was later shredded by strike-slip faults (Sengör et al., 1993; Sengör and Natal'in, 1996). An archipelago model was alternatively proposed (Filipova et al., 2001; Xiao et al., 2008); it consists of accreted and laterally docked pairs of associated accretionary complexes and magmatic arcs. A remarkable feature of the Altaids is the presence of horseshoe-shaped belts, such as the Kazakh Orocline (Fig. 1b; Abrajevitch et al., 2008), or the Central Mongol Orocline (Yakubchuk et al., 2008). These structures are intimately associated with lithosphere-scale strike-slip faults along which palaeomagnetic evidence document block rotations and displacements over thousands kilometres (Van der Voo et al., 2006; Wang et al., 2007; Choulet et al., in press); however, the link between oroclinal bending, transcurrent faulting and accretion remains poorly understood.

This study deals with the structural pattern of the Late Palaeozoic West Karamay accretionary complex, in order to document transcurrent tectonics and lateral docking. On the basis of new geochronological data and multi-scale structural analysis, we present the first evidence of an oblique convergent system in West Junggar. Considering the structural pattern of the Central Asian puzzle, we discuss the possible origin of oblique subduction, and the controls of regional geodynamics on the geometry of the convergent plate boundary.

2. Geological outline

2.1. Central Asia

In the central part of the Altaids, a region that extends from central Kazakhstan to Xinjiang (northwestern China), three main geological domains are recognized (Fig. 1b). To the northeast, (1) the Altai range is composed by Early and Late Palaeozoic units that were accreted and docked to the Siberian margin and affected by high-grade metamorphism (Windley et al., 2002; Xiao et al., 2004). To the south, the convergence between the Tarim Block and several micro continents such as Yili and Central Tianshan formed the (2) Palaeozoic Tianshan Orogen (Charvet et al., 2007). The central and northwestern parts of Central Asia display a horseshoe shape that can be followed from North Tianshan to West Junggar around the Balkash Lake area (Fig. 1b). This megastructure is termed the (3) Kazakh Orocline (Zonenshain et al., 1990). In central Kazakhstan, the outer part of the orocline is made of micro continents and intra-oceanic arcs, which amalgamated during the Early Palaeozoic (Kröner et al., 2008). In the inner part of the orocline, the subduction of the Junggar Ocean below the Kazakhstan active margin generated Late Palaeozoic accretionary complexes and magmatic arcs (Degtyarev, 1999; Wang et al., 2006; Windley et al., 2007). To the north of this domain (Fig. 1b), the Irtysh-Zaisan fold-and-thrust Belt results from the Late Carboniferous closure of the Ob-Zaisan Ocean that originally separated the Kazakh orocline and the south-western margin of Siberia (Buslov et al., 2004). The Permian-Early Triassic transcurrent tectonics that affected Central Asia (Allen et al., 1995; Laurent-Charvet et al., 2003), eventually dismembered the oroclinal system, displaced segments over more than 1000 km, and thus disorganised its original structure (Wang et al., 2007; Choulet et al., in press).

2.2. West Junggar

West Junggar, a mountainous area located along the Kazakh border in northwestern China, forms the easternmost part of the Kazakh orocline (Fig. 1b). It is limited by two major strike-slip fault systems, the Irtysh-Gornotsaev sinistral shear zone to north and the Chingiz-Alakol-North Tianshan dextral shear zone to the south (Choulet et al., in press; Fig 1b). Permian displacements along these faults have been estimated from several hundreds to more than one thousand kilometres (Wang et al., 2007; Choulet et al., in press). These faults represent major tectonic boundaries between West Junggar, Altai, and Tianshan. Although detailed investigations are rare in West Junggar, several authors have recognized numerous stratigraphic and tectonic units (Feng et al., 1989; Buckman and Aitchinson, 2004). The section below is a brief summary of the litho-stratigraphic units defined in Choulet et al. (unpublished results; Fig. 2a).

The Chingiz-Tarbagatay Unit in the central part of the West Junggar massif, is composed of Early Palaeozoic mélange, turbidite and magmatic arc rocks (Unit I in Fig. 2a; Feng et al., 1989). The Mayila and Tangbale Units are also formed by Early Palaeozoic ophiolitic mélanges and turbidites (Units IVa and IVb in Fig. 2a; Buckman and Aitchinson, 2004). Unconformable Middle Devonian conglomerate that overlie Ordovician and Silurian rocks argue for a Late Silurian event (XBGRM, 1965). A-type Early Devonian granites intrude the Chingiz-Tarbagatay Unit and postdate the pre-Late Silurian accretion-subduction (Chen et al., 2010). These units with still a poorly documented architecture represent the substratum of the Devonian-Carboniferous arcs (Units IIa and IIIa in Fig. 2a). At the end of the Middle Devonian, two new subduction zones developed. To the north, the south-dipping subduction of the Ob-Zaisan Ocean by generated the Sawuer arc and Erquis accretionary complex (Unit IIa and IIb in Fig. 2a; Windley et al., 2007; Shen et al., 2008; Zhou et al., 2008b; Chen et al., 2010). To the south, the Barliek magmatic arc, and the West Karamay accretionary complex are related to the northwest-dipping subduction of the Junggar Ocean (Units IIIa and IIIb in

Fig 2a; Feng et al., 1989; Buckman and Aitchinson, 2004; Chen et al., 2006; Xiao et al., 2008). This magmatic arc–subduction complex assemblage corresponds to the easternmost extension of the Kazakh orocline (Choulet et al., in press; Fig. 1b).

A particularity of West Junggar is the abundant and widespread Late Palaeozoic magmatism (Han et al., 2006; Fig 2a), which affected the entire Central Asia (Jahn et al., 2000). Magmatic suites consist of A-type and I-type plutons, mafic dykes and volcanic rocks, emplaced between 320 Ma and 250 Ma (Chen and Jahn, 2004; Li et al., 2004; Han et al., 2006; Xu et al., 2008; Geng et al., 2009; Yin et al., 2010). A-type granitoids were generated either by a partial melting of the depleted-mantle reservoir (Han et al., 1999) or, alternatively, by a thermally induced melting of the Palaeozoic juvenile lower crust followed by in situ differentiation (Chen and Jahn, 2004; Su et al., 2006); or both processes acting together (Chen and Arakawa, 2005; Geng et al., 2009). I-type granitoids stem from the melting of Early Palaeozoic juvenile crust (Chen and Jahn, 2004) or a depleted mantle reservoir (Zhou et al., 2008b). Dolerite and low-Mg diorite dykes dated between 283Ma and 241Ma (Qi, 1993; Li et al., 2004; Xu et al., 2008; Zhou et al., 2008a) have a depleted-mantle origin. All these rocks have been assigned a post-collisional setting.

In contrast, 320-300 Ma calk-alkaline rocks with adakitic affinities (Zhang et al., 2006; Geng et al., 2009; Tang et al., 2010) and high-Mg diorite dykes (Yin et al., 2010) were recently described and slab melting related to ridge subduction was proposed to account for their genesis. These new data led several authors to consider that subduction may have continued during Permian (Geng et al., 2010; Xiao et al., 2010), but this is not supported by field evidence. Actually, eruption of Permian lava flows (Tan et al., 2006) is closely associated with the accumulation of Permian coarse red sandstones and conglomerates, considered as a post-orogenic molasse (Feng et al., 1989; Allen et al., 1995; Jin and Li, 1999;

Buckman and Aitchinson, 2004; Fig. 2b). Undeformed Early Permian molasse postdates turbidite accumulation; therefore, subduction likely ended before the Early Permian.

All the Palaeozoic rocks of West Junggar have been affected by Permian post accretion transcurrent tectonics (Allen et al., 1995; Laurent-Charvet et al., 2003; Fig 1b). SW-NE trending faults, such as the Dalabute sinistral fault, affect Permian plutons and generate cataclasite (Allen et al., 1995; Fig 2b), whilst ductile mylonite is never observed.

3. Age and nature of the West Karamay Unit

West Junggar Mountains are bounded to the east by the Junggar basin (Fig. 2b); in this area, low elevation and desert morphology expose discontinuous outcrops. From the bottom to the top, the Carboniferous Xibeikulasi, Baogoutu, and Tailegula formations have been classically recognized (XBGRM, 1966; 1978; Wu and Pan, 1991); however, similar lithologies and the lack of accurate stratigraphic evidence led several authors to reappraise this classification (Feng et al., 1989; Buckman and Aitchinson, 2004; Choulet et al., unpublished results). In the following section, they will be collectively termed "West Karamay Unit" (Fig. 2b; Choulet et al., unpublished results). This unit consists of imbricate slices of turbidite, greywacke, and ophiolitic mélange (Feng et al., 1989), described thereafter (Fig 2b).

3.1. The turbidite series

In the West Karamay Unit, ca. 10 m-thick alternations of fine-grained grey siltstone and blackish mudstone are the predominant lithology (Feng et al., 1989; Li and Jin, 1989; Guo et al., 2002; Fig. 3a); in many places, the Permian magmatism and associated high heat flow

transformed these rocks into hornfels (Choulet et al., unpublished results; Fig. 2a). In clastic rocks, quartz and clay are dominant, but many feldspar and lithic clasts are also preserved (Fig. 3b), and coarse-grained, greywacke contains numerous andesite clasts (Fig. 3c). Slumps, disrupted soft sandstone beds, Bouma sequences (Fig 3d), and the coexistence of deep-water and shallow-water ichnofacies attest to the tectonic instability of the basin and resedimentation processes (Jin and Li, 1999).

Rare fossils of plants, corals and brachiopods do not provide a better age assignment than Carboniferous (XBGRM, 1966; Li and Jin, 1989; Wu and Pan, 1991). Recent U-Pb geochronological data on detrital zircons yield a maximum Late Carboniferous age (ca. 305 Ma) for turbidite deposition, which is close to the age of accretion (Choulet et al., unpublished results). The positive εHf values of these zircons argue for a juvenile origin consistent with an immature active margin (Choulet et al., unpublished results). The bedding (S_0) is usually apparent in coarse-grained turbidites, but often undistinguishable from the slaty cleavage (S_1) in black mudstone. Relationships between bedding and cleavage will be described and discussed later in this article. Turbidites often dip steeply, however upright folds hinges are rarely observed (Fig. 3e).

3.2. The graywacke mass flows

Mass flows are lenses without obvious internal structure intercalated within turbidite series (Wu and Pan, 1991; Guo et al., 2002). These discharges of sand-sized volcanic materials can reach tens of metres in thickness. Despite highly variable geometry of the mass flow itself, the greywacke is very homogenous and occasionally well sorted (Guo et al., 2002); quartz, zoned feldspar and volcanic-rock clasts are dispersed in a matrix of fine-grained quartz and clay (Fig. 3f). Rock fragments are usually dark andesite, occasionally exposing fluidal texture

(Fig. 3g), consistent with a volcanic-arc origin for these volcaniclastic rocks. Greywackes are lithologically identical to the volcaniclastic sandstone beds of turbidite sequences. Some of these rocks were previously referred to as volcanic tuffs (Wu and Pan, 1991; Buckman and Aitchinson, 2004), however, the clayey matrix and rounded clasts clearly rule out a pyroclastic origin for this rocks, which otherwise present all the features of volcaniclastic turbidites accumulated in a fore-arc basin. Nevertheless, Tournaisian-Visean and Moscovian volcanic tuffs are locally associated with greywacke mass-flows (Guo et al., 2010; Zhang et al., 2011a), a possible consequence of transient filling-up.

A U-Pb geochronological study on detrital zircons was performed on a sample of greywacke from Sartuohai (Fig. 2a). In coarse-grained greywacke, zircons were separated and analyzed by LA-ICPMS at the Institute of Geology and Geophysics, Chinese Academy of Sciences, Beijing. Details regarding analytical procedure and instrumentation can be found in Wu et al. (2010). Isotopic ratios and individual ages are reported in Table 1. Detrital zircon grains are generally euhedral and display growth zoning on cathodo-luminescence images (Fig. 4a), a feature consistent with a magmatic origin. The U-Pb Concordia plot displays concordant ages, which are considered as crystallization ages (Fig. 4b). The age distribution pattern shows one single population mode of 320 Ma and a maximum age of sedimentation (the mean of the three youngest concordant grains; Dickinson and Gehrels, 2009) of ca. 305 Ma (Fig. 4c).

These results are similar to those obtained from nearby tuff and turbidite (Zhang et al., 2011a; Choulet et al., unpublished results). Each sample of tuff, greywacke and turbidite displays an unimodal age distribution, with a population peak ranging between 330 Ma and 320 Ma (Fig. 4c). Maximum ages of deposition of both turbidites and greywacke mass flows cluster around 305 Ma. The consistency between minimum age of sedimentation and single population peak age implies a local and single source for the turbidites and greywacke

discharges (Zhang et al., 2011a; Choulet et al., unpublished results). This is consistent with the angular shape of detrital zircon grains that indicate short transport from the source to the basin (Fig. 4a). The potential sources of these zircon grains are the mid-Carboniferous (Feng et al., 1989; Han et al., 2006; Shen et al., 2008; Chen et al., 2010) Barliek and Sawuer magmatic arc rocks.

3.3. Ophiolitic and sedimentary mélanges

These rock bodies occur as irregular bands, within the sedimentary series (Fig. 2b). Mélanges are characterized by the lack of internal strata continuity and inclusion of various-sized blocks of oceanic material in a fragmented fine matrix (Greenly, 1919; Raymond, 1984). In West Junggar, the matrix is usually serpentine or, locally, metasomatized serpentine, termed listwaenite (Buckman and Aitchinson, 2004), this material is highly sheared and encloses lens-shaped exotic fragments. Many stripes of mélange interleaved with sediments are too small for being represented on geological maps; in contrast, two large bands, the Dalabute and Karamay mélanges have been mapped in detail (Feng et al., 1989; Zhang et al., 2011a; 2011b; Fig. 2b).

3.3.1. The Dalabute mélange

The Dalabute (also called Darbut) ophiolitic mélange crops out on the northwestern side of the Dalabute Fault (Fig. 2b). The width of the rock body can reach several kilometres and its fabric dips steeply. However, a preserved northwest dipping foliation suggests that the ophiolitic mélange lies below the sediments that crop out to the west of the Dalabute Fault (Feng et al., 1989; Fig 2c).

The mélange also contains serpentinized harzburgite blocks that can reach several tens to hundreds of metres near Sartuohai mine (Fig. 2b; 5a), cumulate gabbro, and basalt metamorphosed into amphibolite or greenschist (Feng et al., 1989; Fig. 5b). Pillow basalts are not uncommon (Fig. 5c). Mafic rocks display OIB, N-MORB or E-MORB affinities (Zhang et al., 1993; Wang et al., 2003; Buckman and Aitchinson, 2004; Lei et al., 2008; Gu et al., 2009; Liu et al., 2009). Since the dismembered nature of the mélange facilitates fluids migration, some magmatic rocks have been transformed into roddingite at the boundary with the serpentinite matrix (Buckman and Aitchinson, 2004; Fig. 5d). The rheological behaviour of serpentinite (Saleeby, 1984) also enhances the exhumation of high-grade metamorphic rocks such as blueschists (Feng et al., 1989). Boulders of red chert and recrystallized radiolarite are often associated with greenish mafic rocks, giving the landscape its typical "coloured mélange" look (Fig. 5e). Sometimes, mixtures of chert, basalt and limestone appear within one single block (Fig. 5f), and this close association is a clear evidence for pre-melange syntectonic sedimentation. Modern analogues of these features can be found at sites of oceanic mantle denudation, such as the Gorringe Bank in the Atlantic Ocean (Lagabrielle and Auzende, 1982).

Olistostromes and broken formations are often closely associated with ophiolitic mélange stripes; they contain intrabasinal dismembered strata, and exotic blocks as well. Various-sized limestone lenses are irregularly distributed along the strike of the Dalabute fault (XBGRM, 1966; Guo et al., 2002; Fig. 5g). This thin-bedded limestone is highly recrystallized, but contains remnants of crinoids and Devonian to Carboniferous rugose corals as well (XBGRM, 1966). The limestone also locally contains gabbro phacoids associated with sandstone, conglomerate and breccia (Fig. 5h), that contain a significant amount of pyroxene, feldspar and gabbro fragments (Fig. 5i). The occurrence of mafic clasts argues for syn-tectonic sedimentation to have occurred prior to accretion. A detailed structural study of this limestone

will be provided in the next section. The sedimentary mélange also contains phacoids of greywacke and turbidite, similar to those of the coherent sedimentary units.

The age of the Dalabute mélange is uncertain since its matrix remains undated. Poorly preserved radiolarian fossils in chert blocks indicate a Middle Devonian age (Feng et al., 1989). Sm/Nd and U-Pb isotopic ages of 395 ± 12 Ma and 391 ± 7 Ma, respectively have been obtained on blocks of oceanic gabbro (Zhang et al., 1993; Gu et al., 2009). An E-MORB leucogabbro yields a zircon U-Pb age of 302 ± 2 Ma (Liu et al., 2009). This age is very close to that of alkaline plutons that obviously postdate mélange emplacement (Geng et al., 2009). Since no information on the sampling location of this leucogabbro is available, this rock could be a boulder within the mélange, or alternatively a dyke or a sill that crosscuts it. Therefore, this date must be considered with caution and will not be used in our discussion.

3.3.2. The Karamay mélange

This stripe of mélange, also called Baijiantan mélange or Baikouquan (Zhu et al., 2008), that crops out at the boundary of the Junggar Basin is partly hidden by Mesozoic sediments (Fig. 2b). Thus, the breadth of the band is possibly underestimated. Geometrically, the Karamay mélange lies below the sedimentary stack; a configuration similar to that of Dalabute mélange (Feng et al., 1989). The matrix of the mélange consists of highly sheared serpentinite, which encloses various-sized blocks of harzburgite, metagabbro, basalt and chert (Fig. 5j, 5k and 5l). Mafic rocks display both OIB and MORB geochemical affinities (Zhu et al., 2007; Zhang et al., 2011b). Metamorphic mineral assemblages representative of pressure up to 27 kbar are preserved within dolomitic marble and garnet amphibolite blocks (Zhu et al., 2008). Exsolution textures in two-pyroxenes lherzolite lenses also attest for high-grade metamorphism and deep burial (Zhu and Xu, 2007).

The formation of the Karamay Mélange is not well time-constrained. Zircons extracted from a gabbro yield two U-Pb ages at 415 ± 8 Ma and 332 ± 14 Ma (Xu et al., 2006), but the significance of these ages is uncertain. Based upon regional correlation, and in agreement with Geng et al. (2009), and Zhang et al. (2011a), we consider that the Late Silurian-Lower Devonian age may come from inherited grains, whilst the Visean age represents the crystallization age of gabbro. Zhu et al. (2007) also provide a zircon U-Pb age of 517 Ma on a pillow basalt of the OIB type; however, this data will not be considered since it is based on one single and highly discordant individual age, only.

3.4. Magmatic and tectonic features of the West Karamay Unit

High-Mg diorite dykes, dated at 321±1 Ma, by ^{40}Ar-^{39}Ar method, were likely formed by partial melting of the mantle metasomatised by slab-derived fluid/melt (Yin et al., 2010). The calk-alkaline plutons of Baogutu porphyry copper belt intrude the West Karamay unit and consist in diorite porphyry stocks that document Late Carboniferous arc magmatism (Shen et al., 2009). 315-310 Ma adakites also crop out in the Baogutu area, and a slab melting origin is forwarded (Tang et al., 2010). Many circular plutons intrude the West Karamay Unit (Kwon et al., 1989; Fig. 2b). The oldest intrusion is dated at 305 ± 5 Ma, but many ages stretch from 300 Ma to 280 Ma (Kwon et al., 1989; Han et al., 1999; 2006; Chen and Jahn, 2004; Su et al., 2006; Geng et al., 2009). Recently, diorites with adakitic affinity were interpreted as the result of the partial melting of a subducted slab (Geng et al., 2009). An alternative origin of these magmas could be a partial melting of the mafic juvenile lower crust consistent with the Permian post-accretionary episode (Jahn et al., 2000). However, the slab melting interpretation (Geng et al. 2009) does not contradict the post-accretionary setting hypothesized for the Late Carboniferous to Permian magmatism, since subduction related

magmas can be retained in the crust during a residence time of several millions years (Wang et al., 2009). Alkaline magmatism persists until the Late Permian, with the emplacement of a doleritic to basaltic dyke swarm (Qi, 1993; Li et al., 2004; Han et al., 2006; Xu et al., 2008; Zhou et al., 2008b).

The West Karamay Unit is divided into two parts by the NE-SW trending Dalabute fault (Fig. 2b). This sinistral fault affects post-accretionary plutons, but estimate of its offset is not available. Strike slip faulting continued in Early Mesozoic time and intensely disturbed the primary Palaeozoic geometry (Allen et al., 1995; Xu et al., 2009). Cenozoic tectonics also reactivated most tectonic discontinuities (Avouac et al., 1993); however, this reactivation remains weak in West Junggar, compared to Tianshan.

4. New structural evidence for transpression

Within the West Karamay Unit, the deformation is irregularly expressed, depending on the lithology and observation scale.

4.1. Mega scale structures of the West Karamay Unit

Mega scale structures are obviously visible on satellite scene (available at https://zulu.ssc.nasa.gov/mrsid/ and http://maps.google.com/; Fig. 6a). Lineament analysis reveals two types of linear structures within the sedimentary series of the West Karamay unit (Fig. 6b). Type 1 lineaments draw kilometre-scale undulations and tens of kilometres wide S-shaped features (Fig. 6a and b) that are interpreted as mega scale drag-folds with vertical axes. Type 2 lineaments display a regular pattern, with two principal directions. To the northwest of the Dalabute Fault, the trend is N100°E, whereas to the southeast of the fault, the

average direction is N75°E. Such a constant distribution pattern suggests that the type 2 lineaments represent the slaty cleavage trend developed in the turbidites.

Field investigations confirm our interpretation of the mega scale structures. At outcrop scale, the bedding S_0 shows a persistent vertical or steep dip, but a frequently changing strike (Fig. 2a; 6c), consistent with the folds with vertical axes inferred from satellite imagery (Fig. 6a). The pervasive slaty cleavage in fine-grained sedimentary rocks displays a constant attitude, which depends upon the location (Fig. 2a; 6d). To the north of Dalabute Fault, the cleavage trend is ca. N110°E, whilst, to the south of the fault, its average trend is ca. N70°E, fully consistent with satellite observation (Fig. 6a; 6b).

Although folds with vertical axes are common geologic features, they may generate through different mechanisms (Reutter et al., 1991; Fig. 7). They may form by tilting or refolding of preexisting upright or recumbent folds (Fig. 7a; 7b). However, the lean by 90° of the whole region would require large detachment structures that are totally lacking in West Junggar. Moreover, there is no progressive change from gently to steeply plunging fold axes. Alternatively, wrench tectonics could directly generate folds with steeply dipping axes (Fig. 7c). Drag folds with oblique to vertical axes appear in brittle or ductile wrench shear zones (Ramsay, 1967; Sanderson, 1979, Berthé and Brun, 1980; Carreras et al., 2005). The steepening of the sedimentary series requires a preliminary deformation stage, which is locally documented in the Karamay Unit (Wu and Pan, 1991; Zhang et al., 2011a; Fig. 3e). A continuum between compression and transpression can also be envisaged and will be discussed later in this paper.

It is worth to note that, on satellite scenes, circular plutons neatly crosscut the two types of lineament (Fig. 6a; 6b), thus clearly demonstrating that Late Carboniferous magmatism postdates the folding. Moreover, near the Dalabute Fault, both bedding and cleavage deflect and progressively become tangent to this NE-SW trending fault (Fig. 6e; 6f).

4.2. Mesoscale and microscale structures in the West Karamay Unit

Since West Junggar rocks do not record significant crust thickening, there is also no evidence for any ductile deformation and high-grade metamorphism. However, our structural investigations reveal that limestone olistoliths, silicified siltstone, well-sorted turbidite, or mafic magmatic rocks record a pervasive deformation restricted to a ca. 4-5 km wide band along the Dalabute Fault.

4.2.1. Polyphase ductile shearing within limestone olistoliths

Several hundred of metres to kilometre-scale massive limestone blocks, which crop out along the northern side of the Dalabute fault zone (XBGRM, 1966; Guo et al., 2002), draw asymmetric S-shaped drag folds (Fig. 8a). The well-defined vertical planar fabric represents both bedding and foliation (Fig. 8b). This $S_{0\text{-}1}$ surface is deformed by three types of folds. Upright or slightly recumbent folds are rarely observed (Fig. 8c). Folds with vertical axes are generally tight or isoclinal (Fig. 8d) and develop a vertical axial plane cleavage striking N80°E (Fig. 8e). Multi-scale (from centimetre to several metres) second-phase gentle to open folds with similarly steeply plunging axes refold the early folds (Fig. 8a; 8f; 8g). An horizontal mineral/stretching lineation (L_1) develops on the $S_{0\text{-}1}$ surface (Fig. 8h).

Limestone blocks are often associated with gabbro and gabbroic sandstone lenses (Fig. 5h; 5i). The sigmoidal shape of these metre-scale phacoids indicates sinistral shearing. Though mafic rocks are too strong to experience ductile deformation, they developed a rough vertical foliation. This planar fabric is deflected at the block boundary, in agreement with a sinistral shearing along a N60°E direction. Microscopic observation in thin sections perpendicular to the foliation and parallel to the lineation (i.e. in the horizontal plane) of limestone and mafic sandstone show asymmetric clasts of calcite, quartz or epidote that indicate a left-lateral

shearing (Fig. 8i; 8j). The sinistral kinematics of the clayey shear bands that develop in sandstone corroborates this interpretation (Fig. 8k).

Both sinistral and dextral asymmetric fold limbs appear in limestone (Fig. 8f; 8g). S-shaped open folds, sheared along N30°E and N80°E directions, are distributed along the fold long limb (Fig. 8f). In contrast, open to gentle Z-shaped drag folds appear with a north-south trend and indicate a dextral sense of shear (Fig .8g). Such a geometry is consistent with a conjugate fault configuration (Riedel, 1929). Considering the N50°E sinistral shearing along the Dalabute Fault, slightly oblique secondary faults with sinistral kinematics may develop along the N°30-N40°E and N°70-80°E directions (R and P-type, respectively, Fig. 8f). The highly oblique dextral faults along the N-S direction may correspond to antithetic shear zones (R'-type; Fig. 8g). The kinematic indications observed around the Dalabute Fault therefore attest for a bulk sinistral shearing.

4.2.2. Evidence for folds with vertical axes in turbidites.

Ductile fabric and kinematic indicators generally lack in massive greywacke, whilst they are widespread in turbidite. In mudstone, a penetrative slaty cleavage (S_1) develops and generally erases or transposes the sedimentary bedding (S_0). In contrast, in coarser-grained well-sorted turbidites, the relationships between sedimentary and tectonic fabrics clearly appear. Both S0 and S1 are steeply dipping, and make an angle that vary from 0° to 90° in the limbs and hinge, respectively (Figs. 9a; 9b and 9c). These metre- to hectometre-scale structures are consistent with the megascale folds with vertical axes, inferred from observation of satellite scenes (Fig. 6a; 6b). The cleavage trend remains relatively constant throughout the West Karamay Unit, except in the vicinity of the Dalabute fault zone, where it has been reoriented parallel to the fault (Fig. 6e). Therefore, the regional cleavage may be

related to the large-scale folds with vertical axes. Metre-scale isoclinal folds with vertical axes also develop in siliceous siltstone of the turbidite series (Fig. 9d and 9e).

5. Discussion

These new structural data raise fundamental questions about the timing and origin of the deformation. In this section, we discuss these two points and, on the basis of preexisting data, we propose a possible scenario for the West Junggar Palaeozoic evolution in the frame of the Central Asia geodynamics.

5.1. The West Karamay Unit: a single Carboniferous accretionary complex

New investigations in West Junggar led us to reconsider the nature and origin of the West Karamay Unit. Dalabute and Karamay ophiolitic mélanges probably formed by off scrapping oceanic crust materials and bathyal sediments from the lower oceanic plate. Both MORB and OIB-like components of the mélange (Zhang et al., 1993; Wang et al., 2003; Zhu et al., 2007; Lei et al., 2008; Gu et al., 2009; Liu et al., 2009; Zhang et al., 2011b) argue for an oceanic basin (e.g. oceanic crust and seamounts). Pre-subduction features, such as ophiolitic detritism, are commonly preserved, but the initial oceanic stratigraphy is completely disturbed (Fig. 5f; Feng et al., 1989). Rheologically contrasted oceanic materials generate the disrupted aspect of the mélange and allow strain partitioning (Fig. 5a; 5b; 5d; 5j; 5k). Serpentinite is especially ductile, even at a low temperature, and may accommodate the bulk of deformation both by plasticity and protrusion processes (Saleeby et al., 1984). Boulders of high-strength rocks such as gabbro, basalt, and chert, generally preserve their initial magmatic or sedimentary structure, and are only deformed at their boundaries (Fig. 5b; 5d; 5j; 5k). However, at high

strain rates, phacoids (lens-shaped boulders) are not uncommon. The local occurrence of high-grade rocks (eclogite and blueschist; Feng et al., 1989; Zhu and Xu, 2007; Zhu et al., 2008), in spite of an overall greenschist facies, is probably due to the syntectonic exhumation of the deepest parts of the West Karamay Unit, favored by the ductile flow of serpentinite matrix.

Turbidites, greywacke mass flows and olistostrome formations geometrically overlie the mélange. Although folded and faulted, sedimentary rocks remain coherent, as suggested by type 1 lineaments observed in the satellite images (Fig. 6a). Broken formations, slumps and occurrence of allochthonous limestone boulders suggest a syntectonic sedimentation developed in an unstable margin. Andesite, pyroxene and plagioclase clasts that are widespread in greywacke, turbidite, and mass-flow deposits as well, argue for a nearby volcanic-arc source. Finally, the occurrence of one single detrital population of Late Carboniferous age within sandstone samples of the West Karamay Unit, demonstrates one single and local magmatic-arc source (Fig. 4c).

The association of turbidites, greywacke, mass-flows and ophiolitic mélange in the West Karamay Unit suggest that they formed in an acccretionary complex. Buckman and Aitchinson, (2004), Xiao et al. (2008), and Geng et al. (2009) already proposed this interpretation, and considered that the Karamay Unit was a combination of three separate terranes. They distinguished, i) to the west, the Kulumudi terrane, interpreted as a Devonian accretionary wedge, ii) the Karamay terrane, to the east, corresponding to accreted Carboniferous oceanic material, and iii) the Sartuohai terrane equivalent to the Dalabute mélange and laying in-between the two aforementioned terranes. The Karamay mélange was not included in this tectonic analysis. Recently, Zhang et al., (2011a; 2011b) have suggested that the eastern and western domains represent two separate accretionary complexes formed along two opposite subduction zones. All these models assume that the Dalabute Fault was a

major terrane boundary. Our field investigations reveal that the same lithological succession is exposed on both sides of the Dalabute Fault. Moreover, evidence of opposite senses of subduction is unclear, since the transcurrent deformation erased most of the initial structure. Furthermore, the available geochronological data do not confirm the existence of two diachronous accretionary complexes; conversely, the eastern and western domains of the fault appear genetically and chronologically related. Detailed mapping several tens of years ago, already established a similarity of the sedimentary rocks on both sides of the Dalabute Fault (XBGRM, 1966). Presently, our lithological, chronological and structural knowledge does not allow us to distinguish the Dalabute and Karamay mélanges, since blocks are similar in age and nature, and display identical tectonic structures. Finally, the apparent difference between Dalabute and Karamay mélanges is only due to the present geometry on both sides of the Dalabute Fault (Fig. 10), as discussed in the next section. Therefore, in contrast with Buckman and Aitchinson (2004) and Zhang et al. (2011a), we consider only one single West Karamay Unit, made of sedimentary series and ophiolitic mélange.

5.2. Timing of the deformation

New U-Pb geochronology on detrital zircons indicates a Late Carboniferous maximum age of deposition of turbidites and greywackes (Fig. 4c; 11; Zhang et al., 2011a; Choulet al., unpublished results); however, sedimentation may have started earlier, possibly as soon as Middle or Late Devonian (XBGRM, 1966; Feng et al., 1989). Since structures in limestone boulders are similar to that of turbidites, the deformation obviously took place after olistostrome accumulation; thus, all the structures described above result from the same tectonic event. Although transcurrent tectonics is prominent throughout the West Karamay Unit, an earlier stage of compressive tectonics is locally preserved (Feng et al., 1989; Wu and

Pan, 1991; Zhang et al., 2011a). In agreement with these authors, in several places such as Sartuohai or Baijiantan, we recognize thrusts and folds that contributed to place the strata into an upright position. Then, various-scale folds with steep axes deformed upright strata under ductile, low temperature rheological conditions. Firstly, isoclinal to tight folds are accompanied by the development of a vertical E-W axial plane cleavage and a shallow dipping lineation (Fig. 8d; 8d), and asymmetrical clasts and intrafolial folds indicate a sinistral sense of shear (Fig. 8i; 8j). Asymmetrical open or kink-like folds commonly follow the early synfolial folds, and developed during the last increments of ductile shearing (Fig. 8f; 8g).

Alkaline plutons, dated at ca. 300 Ma (Han et al., 2006; Geng et al, 2009) postdate both the compressive and the transcurrent structures (Fig. 6a) that appeared after ca. 305 Ma, which is the age of the youngest deformed turbidites. Such a short interval argues for a deformation continuum between the compressional and transcurrent events.

The geometry of the early synfolial folds, the shallow dipping lineation, and the secondary folds (Fig. 8f; 8g), suggest accommodation of movements along a major wrench shear zone, precursor of the Dalabute Fault, whilst the present fault is only a result of minor reactivation in brittle conditions (Fig. 8a). Brittle faulting probably occurred during Permian time, since the Late Permian conglomerate and sandstone that crop out along the fault valley, display evidence for syn-tectonic sedimentation such as tilted blocks (Zhao et al., 1990; Allen et al., 1995). Permian palaeomagnetic data from remagnetised turbidites sampled on both sides of the fault do not reveal any relative block motion (Choulet et al., in press). This means that either the remagnetisation is younger than faulting, or, alternatively, that fault motion was not large enough to be recorded by palaeomagnetic investigation. Therefore, the two domains of the Karamay Unit, lying on both sides of the Dalabute Fault, initially formed a single continuous domain, and Dalabute and Karamay mélanges originally formed one single belt,

overlain by disrupted sediments. The present-day offset between the two mélanges can be estimated at ca. 110 km (Fig. 10); this bulk value includes the Permian displacements, and possible younger reactivations, as well (Gu et al., 2009).

In summary, two tectonic events may be distinguished in the Karamay Unit (Fig. 11). From 340 Ma to 305 Ma, oceanic material derived from the Devonian Junggar Ocean was scraped-off and accreted in the wedge. Meanwhile, magmatic-arc rocks intruded the Early Palaeozoic substratum or erupted upon it. The accretionary complex was also intruded by 320-300 Ma diorites with adakitic affinities (Geng et al., 2009; Tang et al., 2010; Yin et al., 2010). These authors propose that ridge subduction might have provoked the "unzipping" of the divergent plate boundary (Thorkelson, 1996) and the opening of a slab window (Dickinson and Snyder, 1979). In response, asthenosphere upwelling triggered slab melting, and generated adakitic magma (Kay et al., 1993) in the fore-arc region (Marshak and Karig, 1977; Delong et al., 1979; Hole et al., 1991). Eroded volcaniclastic material fed the fore-arc basin and the accretionary wedge, where they formed syntectonic turbidites and mass-flow deposits. The occurrence of sub-contemporaneous upright folds and folds with vertical axes during the 305-300 Ma interval suggests transpression coeval with oblique accretion in the West Karamay Unit. The 305-300 Ma period also represents the transition from accretion to post-accretion setting. During this period, both alkaline and calk-alkaline magmatic rocks are recorded (Geng et al., 2009; Fig. 10), but no evidence of a Permian subduction can be found in the sedimentary and tectonic records, as well (Feng et al., 1989; Buckman andAitchinson, 2004). Permian brittle transcurrent tectonics coexists with molasse deposition and alkaline magmatism (Fig. 10). In contrast with Tianshan and Altai regions, where Permian post-accretion plutons display the features of synkinematic intrusions, controlled by strike-slip shear zones (Laurent-Charvet et al., 2003; Wang et al., 2009; Pirajno, 2010), West Junggar

plutons do not present fabrics related to a syntectonic emplacement. This may infer either a post-kinematic intrusion, or, alternatively, shallow level emplacement.

The lack of continuity of the West Karamay Unit and Dalabute Fault along strike prevents any accurate calculation of the bulk offset. A series of NW-SE trending strike-slip faults hinders the relationship between the West Karamay Unit and the Early Palaeozoic Mayila Unit. In addition, the connection between the West Karamay Unit and the Early Palaeozoic basement is also unknown, since the deeper parts of the accretionary complex have not been exhumed yet.

5.3. Oblique subduction driven by oroclinal bending

Transpression within an accretionary complex evokes oblique subduction (McCaffrey, 1992). Decoupling of oblique plate convergence into a normal component and a shear component could explain the coexistence of compressive and transcurrent tectonics. Such tectonics features are documented in South America or New Zealand (Reutter et al., 1991; Henderson, 1987). These authors recognized en-echelon fault systems and vertical folds that superimposed on compressive episodes in connection with oblique subduction. Considering these analogues, we suggest that the West Karamay Unit also formed during oblique subduction.

This interpretation raises the issue of oblique subduction inception. Oblique subduction may result either from a changing lower plate vector, or, alternatively, from a modification of the geometry at the boundary between the upper and lower plates (McCaffrey, 1992). Constraints are not available to check the first option, since the oceanic domains completely disappeared by subduction. The second option could account for the development of an oblique convergence in West Junggar. The West Junggar magmatic arc and the accretionary complex can be extended westward into the Kazakh orocline (Fig. 1b). A complex evolution

of this megastructure is documented by the palaeomagnetic data obtained in the three segments of the orocline (Abrajevitch et al., 2007; 2008; Levashova et al., 2003; 2009). Since Late Devonian time, the convergence of Tarim and Siberia caused a bending of the NW-SE trending Middle Devonian active margin (Abrajevitch et al., 2008). In response to this buckling, the magmatic arc segmented into three parts that formed the Kazakh orocline (Fig. 12). These three segments rotated around a vertical axis during the tightening that led to the closure of the Junggar Ocean. A continuous subduction until the Late Carboniferous eventually closed the internal oceanic domain (Abrajevitch et al., 2008).

In order to relate this geodynamic scenario with the structural observations and to explain how oroclinal bending controlled the development of the tectonic features, we propose a comparison with Cenozoic to modern active margins. According to Beck et al. (1994), the association of an oblique subduction with the convex shape of Western North America plate toward the Pacific Plate has strongly favoured the lateral displacement since at least Mesozoic times. In contrast, the oceanward concave shape of the South American plate characterized the configuration of the Bolivian orocline that inhibited or at least limited sideways transports. However, oblique slip was accommodated by internal transpression in the accretionary complex and in the magmatic arc (Reutter et al., 1991; McCaffrey, 1992). In comparison, until the Late Carboniferous (ca. 305 Ma; Fig. 12), West Junggar, affixed to the bend structure of the Kazakh orocline, constituted its easternmost extension. The horseshoe shape, deduced from the available palaeomagnetic data, suggests an oceanward concave active margin (Abrajevitch et al., 2008; Fig. 12). Since relative rotations of the arms, at the lithosphere scale can reach several tens of degrees, the subduction vector with respect to the plate margin changed during the Late Devonian and Carboniferous. During this period, ridge subduction likely occurred, and the resulting slab window probably enabled emplacement of adakitic magma in the fore-arc region (Geng et al., 2009; Tang et al., 2010; Yin et al., 2010).

The “unzipping” of the ridge during subduction can also facilitate transcurrent deformation in the overriding plate (Thorkelson, 1996). Since no lateral displacements in the upper plate are documented, we propose that the concavity of the subduction zone with respect to the oceanic plate generated a transform margin, and a configuration similar to the Bolivian Orocline (Beck et al., 1994). In response, folds with vertical axis developed in West Junggar (Fig. 12). Since the Ob-Zaisan Ocean (that originally separated West Junggar and Siberia during the Palaeozoic) closed in Late Carboniferous time (Windley et al., 2007), the northern segment of the orocline was at that time, affixed to Siberia. This probably played the role of a buttress (Beck, 1991) and hindered the localization of the transcurrent deformation along strike-slip faults.

During the latest Carboniferous (ca. 305-300 Ma), subduction partly ended around the orocline, which had reached ca. fifty per cent of the present curvature only (Abrajevitch et al., 2008). The additional fifty per cent of buckling are supposed to be due to large-scale Permian block rotations along major shear zones (Van der Voo et al., 2006; Abrajevitch et al., 2008; Wang et al., 2007; Choulet et al., in press; Fig. 12). This transcurrent episode partly dismembered the horseshoe. At that time, West Junggar was separated from the northeastern segment of the orocline by the Chingiz-Alakol-North Tianshan fault. The resulting Permian counterclockwise rotation of West Junggar with respect to Kazakhstan probably increased the obliquity of the convergence and modified the shape of the active margin (Choulet et al., in press; Fig. 12). The new Permian convex shape of the convergence zone towards the Junggar microcontinent may have initiated transcurrent displacements along the Dalabute Fault, and duplication of the accretionary complex (Fig. 12).

In this study, we have considered that the basement of the Junggar basin was a microcontinent, but we do not want to speculate much about its nature. Many hypotheses have been proposed, like a trapped oceanic basin (Hsü, 1989; Carroll et al., 1990), a

Precambrian crust (Wu, 1987; Chen et al., 2002), or a Palaeozoic juvenile crust (Chen and Jahn, 2004; Hu et al., 2000). Here, we assume that the Junggar microcontinent is a composite consolidated tectonic block and not a Precambrian craton. However, our results can suggest an alternative origin for the Carboniferous magmatic arc-rocks and accreted materials, drilled below the Mesozoic infill of the Junggar basin (Zheng et al, 2007). Until now, these rocks were hypothesized to belong to an arc-accretionary complex system, independent of the West Karamay Unit (Zhang et al., 2011a; 2011b) that collided with the West Junggar margin. Alternatively, based on our observations in the West Karamay Unit, we suggest that the units hidden below the Junggar basin are equivalent to the West Karamay and Barliek Units, and therefore, are fragments of the same Late Palaeozoic subduction-accretion complex. The present-day geometry is related to major Permian strike-slip faults, such as the Dalabute Fault that transported magmatic-arc rocks and accreted units along the margin. This model is in agreement with that of Wang et al. (2003) who proposed that West Junggar results of the lateral imbrication of a shredded single Palaeozoic active margin. However, our observations only document Carboniferous and Permian "Sunda-style" tectonics, and there is no evidence for such a similar continuous tectonics since the Early Palaeozoic.

This article only focuses on the prominent tectonic features of the accretionary complex, and we did not consider the tectonic response of the magmatic arc to oblique convergence. However, the thermal softening of the lithosphere in the magmatic arc region probably favoured transcurrent deformation of the upper plate (Beck, 1983).

6. Conclusion

This study emphasizes the role of the transcurrent tectonics that affected West Junggar during the Late Palaeozoic. The tectonic structures at various scales include folds with

vertical axes and strike-slip faults that can be interpreted as the tectonic response of the accretionary complex to the forces acting at the boundary between the West Junggar and Junggar oceanic plates. The geometry and kinematics indicators suggest an oblique slip of the lower oceanic plate. Ridge subduction, traced by the adakitic rocks also supports oblique geometry. Non-frontal subduction directly results from the formation of the Kazakh orocline that provoked the bending of the subduction zone and subsequent block rotations. This specific tectonic setting controlled the style of deformation and strain partitioning, with two consecutive episodes of folding and strike-slip faulting.

These tectonic events have deeply altered the original geometry of the accretionary complex, and reorganized the West Karamay unit. The ca. 100 km lateral displacement is responsible for the partial duplication of the accretionary complex, the thickness of which is probably overestimated.

In West Junggar, and in Central Asia as a whole, the production of juvenile crust accounts for vertical growth of the continents (Jahn et al., 2000; Jahn, 2004; Han et al., 2006). Nevertheless, as suggested by Xiao et al. (2010), the continental crust growth in the Altaids is a combination of both lateral and vertical processes. Vertical addition of mantle-derived magmas contributed to the formation of the juvenile continental crust, but lateral transport by strike-slip faults of this newly formed crustal material reorganized the primary tectonic pattern formed during accretion. Although the geological data gathered during the last two decades are not consistent with one single long-lived subduction, the collage model proposed by Sengör et al. (1993), which emphasized the importance of the lateral tectonic transport, remains still valid for the Late Palaeozoic evolution of the Altaids.

Aknowledgements

We thank Xiao Wenjiao and two anonymous referees for their critical reviews, which substantially improved the manuscript. This work was funded by Chinese National SandT Major Project (2011ZX05008) and National Basic Research Program of China (973 Project N° 2009CB825008).

References

Abrajevitch, A.A., Van der Voo, R., Bazhenov, M.L., Levashova, N.M., McCauseland, P., 2008. The role of the Kazakhstan orocline in the late Paleozoic amalgamation of Eurasia. Tectonophysics 455, 61-76.

Abrajevitch, A.A., Van der Voo, R., Levashova, N.M., Bazhenov, M.L., 2007. Paleomagnetic constraints on the paleogeography and oroclinal bending of the Devonian volcanic arc in Kazakhstan. Tectonophysics 441, 67-84.

Allen, C.R., 1965. Transcurrent faults in continental areas - A symposium on continental drift. Philosophical Transaction of the Royal Society London serie A 258, 82-89.

Allen, M.B., Sengör, A.M., Natal'in, B.A., 1995. Junggar, Turfan and Alakol basins as Late Permian to Early Triassic extensional structures in a sinistral shear zone in the Altaid orogenic collage, Central-Asia. Journal of the Geological Society of London 152, 327-338.

Avouac, J-P., Tapponnier, P., Bai, M., You, H., Wang, G., 1993. Active thrusting and folding along the northern Tien-Shan and Late Cenozoic rotation of the Tarim relative to Dzungaria and Kazakhstan. Journal of Geophysical Research 98, 6755-6804.

Beck, M.E., 1980. Paleomagnetic record of plate-margin tectonic processes along the western edge of North America. Journal of Geophysical Research 85, 7115-7131.

Beck, M.E., 1983. On the mechanism of tectonic transport in zones of oblique subduction. Tectonophysics 93, 1-11.

Beck, M.E., 1986. Model for late Mesozoic-early Tertiary tectonics of coastal California and western Mexico, and speculations on the origin of the San Andreas fault. Tectonics 5, 49-64.

Beck, M.E., 1991. Coastwise transport reconsidered: Lateral displacements in oblique subduction zones, and tectonic consequences. Physics of the Earth and Planetary Interiors 68, 1-8.

Beck, M.E., Burmester, R.R., Drake, R.E., Riley, P.D., 1994. A tale of two continents: Some tectonic contrasts between the central Andes and the North American Cordillera, as illustrated by their paleomagnetic signatures. Tectonics 13, 215–224.

Berthé, D., Brun, J-P., 1980. Evolution of folds during progressive shear in the South Armorican Shear Zone, France. Journal of Structural Geology 2, 127-133.

Buckman, S., Aitchison, J.C., 2004. Tectonic evolution of Paleozoic terranes in West Junggar, Xinjiang, NW China. In: Malpas, J., Fletcher, C.J., Aitchison, J.C. (Eds.), Aspects of the Tectonic Evolution of China.: Geological Society, Special Publication, London 226, 101-129.

Buslov, M.M., Watanabe, T., Fujiwara, Y., Iwata, K., Smirnova, L.V., Safonova, I.Y., Semakov, N.N, Kiryanova, A.P., 2004. Late Paleozoic faults of the Altai region, Central Asia: tectonic pattern and model of formation. Journal of Asian Earth Sciences 23, 655-671.

Carreras, J., Druguet, E., Griera, A., 2005. Shear zone-related folds. Journal of Structural Geology 27, 1229-1251.

Carroll, A.R., Liang, Y.H., Graham, S.A., Xiao, X.C., Hendrix, M.S., Chu, J.C., McKnight, C.L., 1990. Junggar Basin, Northwest China – trapped Late Paleozoic ocean. Tectonophysics 181, 1–14.

Chamot-Rooke, N., Rabaute, A., 2007. Plate tectonic from space. Episodes 30, 119-124.

Charvet, J., Shu, L.S., Laurent-Charvet, S., 2007. Paleozoic structural and geodynamic evolution of eastern Tianshan (NW China): welding of the Tarim and Junggar plates. Episodes 30, 162-186.

Chemenda, A., Lallemand, S., Bokun, A., 2000. Strain partitioning and interplate friction in oblique subduction zones: Constraints provided by experimental modeling. Journal of Geophysical Research 105, 5567-5581.

Chen, B., Arakawa, Y., 2005. Elemental and Nd-Sr isotopic geochemistry of granitoids from the West Junggar foldbelt (NW China), with implications for Phanerozoic continental growth. Geochimica et Cosmochimica Acta 69, 1307-1320.

Chen, B., Jahn, B.M., 2004. Genesis of post-collisional granitoids and basement nature of the Junggar Terrane, NW China: Nd-Sr isotope and trace element evidence. Journal of Asian Earth Sciences 23, 691-703.

Chen, J.F., Han, B.F., Ji, J.Q., Zhang, L., Xu, Z., He, G.Q., Wang, T., 2010. Zircon U-Pb ages and tectonic implications of Paleozoic plutons in northern West Junggar, North Xinjiang, China. Lithos 115, 137-152.

Chen, Y., Sun, M.S., Zhang, X.L., 2006. SHRIMP U–Pb dating of zircons from quzrtz diorite at the southeast side of the Baerkule fault, western Junggar, Xinjiang. China. Geological Bulletin of China 25, 992–994.

Chen, X., Lu, H.F., Shu, L.S., Wang, H.M., Zang, G.Q., 2002. Study on tectonic evolution of Junggar Basin, Geological Journal of China Universities 8, 257-267.

Choulet, F., Chen, Y., Wang, B., Faure, M., Cluzel, D., Charvet, J., Lin, W., Xu, B., (in press). Late Palaeozoic palegeographic reconstruction of western Central Asia based upon paleomagnetic data and its geodynamic implications. Journal of Asian Earth Sciences, doi:10.1016/j.jseaes.2010.07.011.

Coney, P.J., Jones, D.L., Monger, J.W., 1980. Cordilleran suspect terranes. Nature 288, 329-333.

Degtyarev, K.E., 1999. Tectonic Evolution of the early Paleozoic Active Margin in Kazakhstan. Nauka, Moscow 123 pp.

DeLong, S.E., Schwarz, W.M., Anderson, R.N., 1979. Thermal effects of ridge subduction. Earth Planetary Science Letters 44, 239-246.

Dickinson, W.R., Gehrels, G.E., 2009. U-Pb ages of detrital zircons in Jurassic eolian and associated sandstones of the Colorado Plateau: Evidence for transcontinental dispersal and intraregional recycling of sediment. Geological Society of America Bulletin 121, 408-433.

Dickinson, W.R., Snyder, W.S., 1979. Geometry of subducted slabs related to San Andreas transform. Journal of Geology 87, 609-627.

Ekström, G., Engdahl, E.R., 1989. Earthquake Source Parametres and Stress Distribution in the Adak Island Region of the Central Aleutian Islands, Alaska. Journal of Geophysical Research 94, 15499-15519.

Engebretson, D.C., Cox, A., Gordon, R.G., 1985. Relative motion between oceanic and continental plates in the Pacific basin Geological Society of America Special Paper 206, 59 pp.

Feng, Y., Coleman, R.G., Tilton, G., Xiao, X., 1989. Tectonic evolution of the West Junggar region, Xinjiang, China. Tectonics 8, 729-752.

Fillippova, I.B., Bush, V.A., Didenko, A.N., 2001. Middle Paleozoic subduction belts: The leading factor in the formation of the Central Asian fold-and-thrust belt. Russian Journal of Earth Sciences 3, 405–426.

Fitch, T.J., 1972. Plate convergence, transcurrent faults and internal deformation adjacent to Southwest Asia and the Western Pacific. Journal of Geophysical Research 77, 4432- 4460.

Geng, H.Y., Sun, M., Yuan, C., Xiao, W.J., Xian, W.S., Zhao, G.C., Zhang, L.F., Wong, K., Wu, F.Y., 2009. Geochemical, Sr-Nd and zircon U-Pb-Hf isotopic studies of Late Carboniferous magmatism in the West Junggar, Xinjiang: Implications for ridge subduction? Chemical Geology 266, 373-398.

Goldfinger, C., Kulm, L.D., Yeats, R.S., Hummon, C., Huftile, G.J., Niem, A.R., McNeil, L.C., 1996. Oblique strike-slip faulting of the Cascadia submarine forearc: The Daisy Bank fault zone off central Oregon. In: Bebout G.E., Scholl D., Kirby S., Platt J.P., Subduction top to bottom - AGU Geophysical Monograph, Washington D.C. 96, 65-74.

Greenly, E., 1919. The Geology of Anglesey. Memoirs of the Geological Survey of Great Britain, London 78, 980 pp.

Gu, P.Y., Li, Y.J., Zhang, B., Tong, L.L., Wang, J.N., 2009. LA-ICP-MS zircon U–Pb dating of gabbro in the Darbut ophiolite, western Junggar, China. Acta Petrologica Sinica 25, 1364-1372.

Guo, H.L., Zhu, R.K., Shao, L.Y., He, D.B., Luo, Z., 2002. Lithofacies palaeogeography of the Carboniferous in the northwest of China. Journal of Paleogeography 4, 25-35.

Guo, L.S., Liu, Y.L., Wang, Z.H., Song, D., Xu, F.J., Su, L., 2010. The zircon U-Pb LA-ICP-MS geochronology of volcanic rocks in Baogutu areas, western Junggar. Acta Petrologica Sinica 26, 471–477.

Han, B.F., He, G.Q., Wang, S.G., 1999. Postcollisional mantle-derived magmatism, underplating and implications for basement of the Junggar Basin. Science in China, Series D 42, 114-119.

Han, B.F., Ji, J.Q., Song, B., Chen, L.H., Zhang, L., 2006. Late Paleozoic vertical growth of continental crust around the Junggar Basin, Xinjiang, China (Part I) : Timing of post-collisional plutonism. Acta Petrologica Sinica 22, 1077-1086.

Henderson, R.A., 1987. An oblique subduction and transform faulting model for the evolution of the Broken River Province, northern Tasman Orogenic System. Australian Journal of Earth Sciences 34, 237-249.

Hole, M.J., Rogers, G., Saunders, A.D., Storey, M., 1991. Relation between alkalic volcanism and slab window formation. Geology 19 657-660.

Hsu, K.J., 1989. Relict back-arc basins: principles of recognition and possible new examples from China. In: Kleinspehn, K.L., Paola, C. (Eds.), New Perspectives in Basin Analysis, Springer, New York 245–263.

Hu, A.Q., Jahn, B.M., Zhang, G.X., Chen, Y.B., Zhang, Q.F., 2000. Crustal evolution and Phanerozoic crustal growth in northern Xinjiang: Nd isotopic evidence. Part I. Isotopic characterization of basement rocks. Tectonophysics 328, 15-51.

Jahn, B.M., 2004. The Central Asian Orogenic Belt and growth of the continental crust in the Phanerozoic In: Malpas, J., Fletcher, C.J., Aitchison, J.C. (Eds.), Aspects of the Tectonic Evolution of China.: Geological Society, Special Publication, London 226, 73-100.

Jahn, B.M., Wu, F.Y., Chen, B., 2000. Massive granitoid generation in Central Asia: Nd isotope evidence and implications for continental growth in the Phanerozoic. Episodes 23, 82-92.

Jarrard, R.D., 1986. Terrane motion by strike-slip faulting of forearc slivers. Geology 14, 780-783.

Jin, H.J., Li, Y.C., 1999. Carboniferous biogenic sedimentary structures on the northwestern margin of Jungar Basin. Chinese Science Bulletin 44, 368-368.

Karig, D.E., Anderson, R.N., Bibee, L.D., 1978. Characteristics of back-arc spreading in the Mariana trough. Journal of Geophysical Research 83, 1213–1226.

Katili, J.A., 1970. Large transcurrent faults in Southeast Asia with special reference to Indonesia. Geologische Rundschau 59, 581-600.

Kay, S.M., Ramos, V.A., Marquez, M., 1993. Evidence in Cerro Pampa volcanic rocks for slab-melting prior to ridge-trench collision in southern South America. Journal of Geology 101, 703-714.

Kimura, G., 1986. Oblique subduction and collision: forearc tectonics of the Kuril Arc. Geology 14, 404–407.

Kröner, A., Hegner, E., Lehmann, B., Heinhorst, J., Windgate, M.T., Liu, D.Y., Erlemov, P., 2008. Palaeozoic arc magmatism in the Central Asian Orogenic Belt of Kazakhstan: SHRIMP

zircon ages and whole-rock Nd isotopic systematics. Journal of Asian Earth Sciences 32, 118-130.

Kusky, T.M., Bradley, D.C., Haeussler, P., 1997a. Progressive deformation of the Chugach accretionary complex, Alaska, during a Paleogene ridge-trench encounter. Journal of Structural Geology, 19, 139-157.

Kusky, T.M., Bradley, D.C., Haeussler, P., Karl, S., 1997b. Controls on accretion of flysch and mélange belts at convergent margins: Evidence from the Chugach Bay thrust and Iceworm mélange, Chugach Terrane, Alaska. Tectonics 16, 855-878.

Kwon, S.T., Tilton, G.R., Coleman, R.G., Feng, Y., 1989. Isotopic studies veering on the tectonics of the West Junggar region, Xinjiang, China. Tectonics 8, 719-727.

Lagabrielle, Y., Auzende, J.M., 1982. Active in situ disaggregation of oceanic crust and mantle on Gorringe Bank: analogy with ophiolitic massives. Nature 297, 490-493.

Lallemand, S., Liu, C.S., Dominguez, S., Schnürle, P., Malavieille, J., and the ACT scientific crew, 1999. Trench-parallel stretching and folding of forearc basins and lateral migration of the accretionary wedge in the southern Ryukyus: a case of strain partition caused by oblique convergence. Tectonics 18, 231-247.

Laurent-Charvet, S., Charvet, J., Monié, P., Shu, L.S., 2003. Late Paleozoic strike-slip shear zones in eastern central Asia (NW China): New structural and geochronological data. Tectonics 22, 1009-1034.

Lei, M., Zhao, Z.D., Hou, Q.Y., Zhang, H.F., Xu, J.F., Chen, Y.L., Zhang, B.R., Liu, X.J., 2008. Geochemical and Sr-Nd-Pb istopic characteristics of the Dalabute ophiolite, Xinjiang: comparison between the Paleo-Asian ocean and the Tethyan mantle domains. Acta Petrologica Sinica 24, 661-672.

Levashova, N.M., Degtyarev, K.E., Bazhenov, M.L., Collins, A.Q., Van der Voo, R., 2003. Permian paleomagnetism of East Kazakhstan and the amalgamation of Eurasia. Geophysical Journal International 152, 677-687.

Levashova, N.M., Van der Voo, R., Abrajevitch, A.V., Bazhenov, M.L., 2009. Paleomagnetism of mid-Paleozoic subduction-related volcanics from the Chingiz Range in NE Kazakhstan: The evolving paleogeography of the amalgamating Eurasian composite continent. Geological Society of America Bulletin 121, 555-573.

Li, J.Y., Jin, H.J., 1989. The trace fossils discovery and its environment significance in Carboniferous turbidite series, the northwest border of Zhunga'er basin, Xinjiang. Scientia Geologica Sinica 63, 9-15.

Li, X.Z., Han, B.F., Ji, J.Q., Li, Z.H., Liu, Z.Q., Yang, B., 2004. Geology, geochemistry and K-Ar ages of the Karamay basic-intermediate dike swarm from Xinjiang, China. Geochimica 33, 574-584.

Liu, X.J., Xu, J.F., Wang, S.Q., Hou, Q.Y., Bai, Z.H., Lei, M., 2009. Geochemistry and dating of E-MORB type mafic rocks from Dalabute ophiolite in West Junggar, Xinjiang and geological implications. Acta Petrologica Sinica 25, 1373-1389.

Malod, J.A., Komar Karta, Beslier, M.O., Zen Jr, M.T., 1995. From normal to oblique subduction: Tectonic relationships between Java and Sumatra. Journal of Southeast Asian Earth Sciences 12, 85-93.

Marshak, R.S., Karig, D.E., 1977. Triple junctions as a cause for anomalously near-trench igneous activity between the trench and volcanic arc. Geology 5, 233-2.

Martinez, A., Malavieille, J., Lallemand, S., Collot, J-Y., 2002. Partition de la déformation dans un prisme d'accrétion sédimentaire en convergence oblique; approche expérimentale. Bulletin de la Société Géologique de France 173, 17-24.

McCaffrey, R., 1991. Slip vectors and stretching of the Sumatran fore arc. Geology 19, 881-884.

McCaffrey, R., 1992. Oblique Plate Convergence, Slip Vectors, and Forearc Deformation. Journal of Geophysical Research 97, 8905-8915.

Mossakovsky, A.A., Ruzhentsev, S.V., Samygin, S.G., Kheraskova, T.N., 1993. Central Asian fold belt: geodynamic evolution and history of formation. Geotectonics 6, 3-33.

Pirajno, F., 2010. Intracontinental strike-slip faults, associated magmatism, mineral systems and mantle dynamics: examples from NW China and Altay-Sayan (Siberia). Journal of Geodynamics 50, 325-346.

Platt, J.P., 1993. Mechanics of oblique convergence. Journal of Geophysical Research 98, 16,239-16,256.

Qi, J.Y., 1993. Geology and genesis of dike swarms in western Junggar, Xinjiang, China. Acta Petrologica Sinica 9, 288–299.

Ramsay, J., 1967. Folding and Fracturing of Rocks. New York: McGraw-Hill.

Raymond, L.A., 1984. Classification of melanges. In: Raymond, L.A. (ed.) Melanges: Their nature, origin and significance. Geological Society of America Special Publication 198, 7-20.

Reutter, K-J., Scheuber, E., Helmcke, D., 1991. Structural evidence of orogen-parallel strike-slip displacements in the North Chilean Precordillera. Geologische Rundschau 80, 135-153.

Riedel, W., 1929. Zur mechanik geologisher brucherscheinungen. Zentralblatt fur Mineralogie, Geologie und Paleontologie B 354-368.

Roeske, S.M., Snee, L.W., Pavlis, T.L., 2003. Dextral-slip reactivation of an arc-forearc boundary during Late Cretaceous-Early Eocene oblique convergence in the northern Cordilera. In: Sisson, V.B., Roeske, S.M., Pavlis, T.L. (eds.), Geology of a transpression orogen developed during ridge-trench interaction along the North Pacific margin. Geological Society of America Special Paper 371, 141-169.

Saleeby, J.B., 1984. Tectonic significance of serpentinite mobility and ophiolitic melange. In: Raymond, L.A. (ed.) Melanges: Their nature, origin and significance. Geological Society of America Special Paper 198, 153-168.

Sanderson, D.J., 1979. The transition from upright to recumbent folding in the Variscan fold belt of southwest England: a model based on the kinematics of simple shear. Journal of Structural Geology 1, 171-180.

Sengör, A.M., Natal'in, B.A., 1996. Paleotectonics of Asia: fragments of synthesis. In: Yin, A. Harrison, M. (Eds.) The Tectonic Evolution of Asia. Cambridge University Press 486-640

Sengör, A.M., Natal'in, B.A., Burtman, V.S., 1993. Evolution of the Altaid tectonic collage and Paleozoic crustal growth in Eurasia. Nature 364, 299-307.

Shen, P., Shen, Y.C., Liu, T.B., Li, G.M., Zeng, Q.D., 2008. Geology and geochemistry of the Early Carboniferous Eastern Sawur caldera complex and associated gold epithermal mineralization, Sawur Mountains, Xinjiang, China. Journal of Asian Earth Sciences 32, 259-279.

Shen, P., Shen, Y., Liu, T., Meng, L., Dai, H., Yang, Y., 2009. Geochemical signature of porphyries in the Baogutu porphyry copper belt, western Junggar, NW China. Gondwana Research 16, 227–242.

Tan, L., Zhou, T., Yuan, F., Fan, Y., Yue, S., 2006. Mechanism of formation of Permian volcanic rocks in Sawu'er region, Xinjiang, China: Constraints from rare earth elements. Journal of Rare Earths 24, 626-632.

Tang, G., Wang, Q., Wyman, D.A., Li, Z.-X., Zhao, Z.-H., Jia, X.-H., Jiang, Z.-Q., 2010. Ridge subduction and crustal growth in the Central Asian Orogenic Belt: evidence from Late Carboniferous adakites and high-Mg diorites in the western Junggar region, northern Xinjiang (west China). Chemical Geology 277 281–300.

Thorkelson, D.J., 1996. Subduction of diverging plates and the principles of slab window formation. Tectonophysics 255, 47–63.

Van der Voo, R., Abrajevitch, A.V., Bazhenov, M.L., Levashova, N.M., 2008. A Late Paleozoic orocline that developed in the central Asian triangle between the converging Baltica, Siberia and Tarim cratons. 33rd International Geological Congress. Oslo.

Van der Voo, R., Levashova, N.M., Skrinnik, L.I., Kara, T.V., Bazhenov, M.L., 2006. Late orogenic, large-scale rotations in the Tien Shan and adjacent mobile belts in Kyrgyzstan and Kazakhstan. Tectonophysics 426, 335-360.

Veevers, J.J., 2003. Pan-African is Pan-Gondwanaland: Oblique convergence drives rotation during 650-500 Ma assembly. Geology 31, 501-504.

Wang, B., Chen, Y., Zhan, S., Shu, L.S., Faure, M., Cluzel, D., Charvet, J., Laurent-Charvet, S., 2007. Primary Carboniferous and Permian paleomagnetic results from the Yili Block (NW

China) and their implications on the geodynamic evolution of Chinese Tianshan Belt. Earth and Planetary Science Letters 263, 288-308.

Wang, B., Cluzel, D., Shu, L.S., Faure, M., Charvet, J., Chen, Y., Meffre, S., de Jong, K., 2009. Evolution of calc-alkaline to alkaline magmatism through Carboniferous convergence to Permian transcurrent tectonics, western Chinese Tianshan. International Journal of Earth Sciences 98, 1275-12987.

Wang, B., Faure, M., Cluzel, D., Shu, L.S., Charvet, J., Meffre, S., Ma, Q., 2006. Late Paleozoic tectonic evolution of the northem West Chinese Tianshan Belt. Geodinamica Acta 19, 237-247.

Wang, Z.H., Sun, S., Li, J.L., Hou, Q.L., Qin, K.Z., Xiao, W.J., Hao, J., 2003. Paleozoic tectonic evolution of the northern Xinjiang, China: geochemical and geochronolgical constrains from the ophiolites. Tectonics 22, 1014.

Windley, B.F., Alexeiev, D., Xiao, W.J., Kröner, A., Badarch, G., 2007. Tectonic models for accretion of the Central Asian Orogenic Belt. Journal of the Geological Society of London 164, 31-47.

Windley, B.F., Kröner, A., Gui, J., Qu, G., Li, Y., Zhang, C., 2002. Neoproterozoic to Paleozoic geology of the Altai orogen, NW China: new zircon age data and tectonic evolution. Journal of Geology 110, 719–737.

Wu, F.Y., Ji, W.Q., Liu, C.Z., Chung, S.L., 2010. Detrital zircon U-Pb and Hf isotopic data from the Xigaze fore-arc basin: Constraints on Transhimalayan magmatic evolution in southern Tibet. Chemical Geology 271, 13-25.

Wu, H., Pan, Z., 1991. Paleozoic sedimentary sequences and their tectonic setting discrimination in Western Junggar, Xinjiang, China. Advances in Geoscience 246-274.

Wu, Q.F., 1987. The Junggar terrane and its significance in the tectonic evolution of the Kazakhstan Plate. Plate Tectonics of Northern China, No. 2, Geological Publishing House, Beijing, pp. 29 – 38.

XBGMR. (1965). Geological map of China, Taleaileke sheet (L-44-23), scale 1:200000.

XBGMR. (1966). Geological map of China, Karamay sheet (K-45-19), scale 1:200000.

XBGMR. (1978). Geological map of China, Toli sheet (L44-24), scale 1:200000.

Xiao, W.J., Han, C.M., Yuan, C., Sun, M., Lin, S.F., Chen, H.L., Li, Z.L., Li, J.L., Sun, S., 2008. Middle Cambrian to Permian subduction-related accretionary orogenesis of Northern Xinjiang, NW China: Implications for the tectonic evolution of central Asia. Journal of Asian Earth Sciences 32, 102–117.

Xiao, W.J., Huang, B.C., Han, C.M., Gun, S., Li, J.L., 2010. A review of the western part of the Altaids: A key to understanding the architecture of accretionary orogens. Gondwana Research 18, 253-273.

Xiao, W.J., Windley, B.F., Badarch, G., Sun, S., Li, J., Qin, K., Wang, Z., 2004. Paleozoic accretionary and convergent tectonics of the southern Altaids: implications for the growth of Central Asia. Journal of the Geological Society 161, 339-342.

Xu, Q.Q., Ji, J.Q., Gong, J.F., Zhao, L., Tu, J.Y., Sun, D.X., Tao, T., Zhu, Z.H., He, G.Q., Hou, J.J., 2009. Structural style and deformation sequence of western Junggar, Xinjiang, since Late Paleozoic. Acta Petrologica Sinica 25, 636-644.

Xu, Q.Q., Ji, J.Q., Han, B.F., Zhu, M.F., Chu, Z.Y., Zhou, J., 2008. Petrology, geochemistry and geochronology of the intermediate to mafic dykes in northern Xinjiang since Late Paleozoic. Acta Petrologica Sinica 24, 977-996.

Xu, X., He, G.Q., Li, H.Q., Ding, T.F., Liu, X.Y., Mei, S.W., 2006. Basic characteristics of the Karamay ophiolitic mélange, Xinjiang and its zircon SHRIMP dating. Geology in China 33, 470–475.

Yakubchuk, A., 2008. Re-deciphering the tectonic jigsaw puzzle of northern Eurasia. Journal of Asian Earth Sciences 32, 82–101.

Yin, J.Y., Yuan, C., Sun, M., Long, X.P., Zhao, G.C., Wong, K.P., Geng, H.Y., Cai, K.D., 2010. Late Carboniferous high-Mg dioritic dikes in Western Junggar, NW China: geochemical features, petrogenesis and tectonic implications. Gondwana Research 17, 145–152. doi:10.1016/j.gr.2009.05.011.

Zhang, C., Zhai, M.G., Allen, M.B., Saunders, A.D., Wang, G.R., Huang, X., 1993. Implications of Paleozoic ophiolites from Western Junggar, NW China, for the tectonics of Central Asia. Journal of the Geological Society of London 150, 551-561.

Zhang, L.C., Wan, B., Jiao, X.J., Zhang, R., 2006. Characteristics and geological significance of adakitic rocks in copper-bearing porphyry in Baogutu, western Junggar. Geology in China 33, 626–631.

Zhang, J., Xiao, W.J., Han, C.M., Ao, S.J., Yuan, C., Sun, M., Geng, H.Y., Zhai, G.C., Guo, Q.Q., Ma, C., 2011a. Kinematics and age constraints of deformation in a Late Carboniferous accretionary complex in Western Junggar, NW China. Gondwana Research 19, 958-974.

Zhang, J., Xiao, W.J., Han, C.M., Mao, Q.G., Ao, S.J., Guo, Q.Q., Ma, C., 2011b. A Devonian to Carboniferous intra-oceanic subduction system in Western Junggar, NW China. Lithos 125, 592-606.

Zhao, X.X., Coe, R.S., Zhou, Y.X., Wu, H.R., Wang, J., 1990. New paleomagnetic results from Northern China – Collision and suturing with Siberia and Kazakhstan. Tectonophysics 181, 43-81.

Zheng, J.P., Sun, M., Zhao, G.C., Robinson, P.T., Wang, F.Z., 2007. Elemental and Sr-Nd-Pb isotopic geochemistry of Late Paleozoic volcanic rocks beneath the Junggar basin, NW China: Implications for the formation and evolution of the basin basement. Journal of Asian Earth Sciences 29, 778-794.

Zhou, J., Han, B.F., Ma, F., Gong, J.F., Xu, Q.Q., Guo, Z.J., 2008a. $^{40}Ar/^{39}Ar$ Geochronology of mafic dykes in north Xinjiang. Acta Petrologica Sinica 24, 997-1010.

Zhou, T.F., Yuan, F., Fan, Y., Zhang, D.Y., Cooke, D., Zhao, G.C., 2008b. Granites in the Sawuer region of the west Junggar, Xinjiang Province, China: Geochronological and geochemical characteristics and their geodynamic significance. Lithos 106, 191-206.

Zhu, Y.F., Xu, X., 2007. Exsolution texture of two-pyroxenes in lherzolite from Baijiangtan ophiolitic melange, western Junggar, China. Acta Petrologica Sinica 23, 1075-1086.

Zhu, Y.F., Xu, X., Chen, B., Xue, Y.X., 2008. Dolomite marble and garnet amphibolite in the ophiolitic melange in western Junggar: Relics of the Early Paleozoic oceanic crust and its deep subduction. Acta Petrologica Sinica 24, 2767.

Zhu, Y.F., Xu, X., Wei, S.N., Song, B., Guo, X., 2007. Geochemistry and tectonic significance of OIB-type pillow basalts in western Mts. of Karamay city (western Junggar), NW China. Acta Petrologica Sinica 23, 1739.

Zonenshain, L.P., Kuzmin, M.I., Natapov, L.M., 1990. Geology of the USSR: a Plate-Tectonic Synthesis. American Geophysical Union, Geodynamic Series 21.

Figure captions

Table 1: La-ICPMS U-Pb detrital zircon data. *: Degree of discordance.

Figure 1: a) location of the Altaids including major cratons and orogenic belts of Eurasia. b) structural map of western Altaids, modified after Windley et al. (2007) and Charvet et al. (2007). The Devonian to Carboniferous Kazakh orocline lying on the pre-Devonian Kazakhstan microcontinent is the major structure of this region. The nature of the microcontinent in the core of the orocline, below the Junggar basin is still controversial, and a discussion on this topic is beyond the scope of this paper. Major faults are also represented. BOLE: Bole Block, CANTF: Chingiz-Alakol-North Tianshan, CKF: Central Kazakhstan Fault, DF: Dalabute Fault, IGSZ: Irtysh-Gornotsaev Shear Zone, MTF: Main Tianshan Fault, NNTL: Nalati-Nikolaiev Teconic Line, TTF: Talas-Fergana Fault.

Figure 2: a) map of West Junggar Mountains, showing the different tectonic units. Two pairs of Late Palaeozoic accretionary complexes and magmatic arcs overlie an Early Palaeozoic substratum, itself formed by arc magmatism and accretion. The location of samples described in this article is also presented. b) structural map of the West Karamay Unit. This unit is in fault contact with the surrounding Barliek, Mayila and Tangbale units. The West Karamay unit is an accretionary complex that comprises Early to Late Carboniferous sedimentary rocks (turbidite series and mass-flow greywacke deposits) and ophiolitic mélanges. The NE-SW trending Dalabute fault separates the unit in two parts. c) geological section across Barliek magmatic arc end West Karamay accretionary complex. P: Permian, Mz-Cz: Mesozoic and Cenozoic sedimentary rocks.

Figure 3: Photographs of turbidites and greywackes from the West Junggar sedimentary units. a: turbidites made of decimetre-scale alternation of medium to coarse-grained volcaniclastc

sandstone (45.9808°N; 85.3093°E), b: microphotographs of lithic, feldspar and quartz clasts within turbidite sandstone (45.7233°N; 84.4516°E), c: fine-grained andesite clast frequently appearing within turbidites (45.7233°N; 84.4516°E), d: syn-sedimentary load casts structures of sandstone-siltstone beds in turbidites (45.8675°N; 84.6934°E), e: upright fold in the turbidites (45.8702°N; 85.2176°E), f: microphotograph of greywacke showing plagioclase, amphibole and pyroxene clasts within a clayey matrix (45.7214°N; 84.4593°E), g: andesite clast with well-expressed fluidal texture in greywacke mass-flow deposit (45.7214°N; 84.4593°E).

Figure 4: a: cathodoluminescence image of representative detrital zircon grains from sample DJ155, showing grain and spot numbers, and $^{206}Pb/^{238}U$ for each analysed spot, b: Concordia plot of U-Pb isotopic ratios from zircons of sample DJ155, c: relative probability diagrams for detrital zircons of samples DJ155, 08YY-02 (Zhang et al., 2011) and DJ15 (Choulet et al., unpublished results).

Figure 5: Photographs of the main lithologies represented within ophiolitic and sedimentary mélanges. a: pyroxenite block within a serpentinite matrix of the Dalabute mélange, near Sartuohai (45.9847°N; 84.9155°E), b: phacoidal blocks of basalts and gabbro, metamorphosed into the greenschist facies, southwest of Sartuohai (45.8698°N; 84.6832°E), c: pillow basalt block, northwest of Sartuohai (46.0895°N; 84.8138°E), d: roddingitized dyke within the Dalabute ophiolitic mélange, along the Dalabute River (45.8609°N; 84.7275°E), e: metric block of red chert within the serpentinite matrix, near Sartuohai (45.9067°N; 84.7743°E), f: mixture of red shale and fine-grained green rocks (probably hyaloclastic basalt), west of Karamay (45.9847°N; 84.9155°E); this facies denotes pre-accretion but syn-tectonic sedimentation upon the oceanic plate (45.7915°N; 84.5622°E), g: decimetre-scale lenses of limestone within the turbiditic sequence, north of Karamay (45.6937°N; 84.8486°E), h: round-shaped block of undeformed gabbro within a strongly deformed limestone lens, west

of Karamay (45.7199°N; 84.4619°E), i: microphotograph of gabbroic sandstone, exposing plagioclase (plg), pyroxene (px) and epidote (ep) angular clasts in a fine-grained matrix of quartz and clay, West of Karamay (45.7199°N; 84.4619°E), j: photograph of horizontal surface, showing vertically dipping schistose serpentinite matrix that supports chert and greenstone boulders, Karamay mélange, north of Karamay (45.9595°N; 84.2975°E), k: sigmoidal block of basalts within the Karamay mélange (45.9595°N; 84.2975°E), l: round-shaped block of gabbro within the serpentinite matrix of the Karamay mélange (45.9595°N; 84.2975°E).

Figure 6: a: satellite map of southeast of West Junggar Mountains (Landsat 7 image downloaded from https://zulu.ssc.nasa.gov/mrsid/mrsid.pl), b: interpretative map of lineaments, with the 2 major trends. Type 1, which is marked by small undulations corresponds to the bedding. Type 2 lineaments display regular N110°E and N80°E trending directions, to the north and to south of Dalabute Fault, respectively. Type 2 linear trend corresponds to the cleavage, c: stereoplot of field measurements of the bedding of the turbidites. Though a preferred NE-SW trending direction is visible, the bedding is variable in trend but constantly dips vertical, d: stereoplot of the cleavage of the turbidite, deduced from field measurements on both sides of the Dalabute Fault. In average, the vertically dipping cleavage is trending N75°E, to the southeast of Dalabute Fault, and N100°E to the northwest of the fault, e: detailed satellite photograph of the northermost part of the West Karamay unit (located in fig. 6b), f: interpretative map of fig. 6e, showing the vertical folds in turbidite. The deflection of the bedding close to the Dalabute Fault is in agreement with a sinistral kinematics.

Figure 7: schematic diagrams showing the three possibilities to generate folds with vertical axes. a: 90° rotation of the fold axis of a preexisting upright fold. b: 90° rotation of both axial plane and fold axis of an early recumbent fold. c: drag folding along a shear zone (e.g.

the Dalabute sinistral strike-slip fault) that induces rotations around a vertical axis of both axial plane and fold axis of a preexisting upright fold.

Figure 8: photographs of structures within limestone olistoliths along the Dalabute Fault. a: Aerial photograph of a deformed limestone lens located in fig. 6b (45.6928°N; 84.4101°E). The general trend of the ribbon is NE-SW and parallels the Dalabute Fault (DF), but, locally, draws S-shaped drag fold consistent with sinistral kinematics along the fault, b: vertically schistosed beds of limestone representing a S0-1 fabric (45.7199°N; 84.4619°E), c: upright to NW verging fold inside limestone (45.7199°N; 84.4619°E), d: horizontal surface exposing isoclinal fold with vertical axis (45.7084°N; 84.4412°E), e: stereoplot showing the vertical axis of the folds and vertical dip of the N80°E trending cleavage within the limestone, f: S-shaped drag fold indicating Riedel P-sinistral shears (45.6928°N; 84.4101°E), g: subsidiary Z-shaped drag fold indicating Riedel R'-dextral shears (45.6928°N; 84.4101°E). The geometric configuration of S and Z-shaped drag folds is consistent with a NE-SW sinistral strike-slip fault, h: horizontal lineation supported by the vertical cleavage of limestone (45.7084°N; 84.4412°E), i: microphotograph of a sigmoid clast of an altered feldspar (fd, 45.6928°N; 84.4101°E), j: microphotograph of a deformed crinoid fragment made of calcite (cc, 45.6928°N; 84.4101°E), k: clayey shear bands indicating (45.5747°N; 84.2464°E). The i, j and k pictures show microstructures documenting sinistral kinematics.

Figure 9: a, b and c: field photographs showing the geometric interactions between the bedding (S0) and the cleavage (S1), with parallel (a), oblique (b) and perpendicular intersections (c), respectively, from northwest of Karamay (45.7777°N; 84.5174°E). The distribution in map of these structures display folds with vertical axes of several metres amplitude. In fig. 8b, the penetrative character of the S1 cleavage depends on the lithology. d and e: examples of 10 cm-scale isoclinal folds with vertical axis developed in silicified siltstones (45.3978°N; 83.4024°E).

Figure 10: a: 3D diagram of the West Karamay unit and surrounding units. Upright and vertical folds, and thrust deform the accretionary complex. These structures are postdated by the Late Carboniferous plutons. Transcurrent events marked by strike-slip fault affected the region, during the Permian. The 110 km of displacement along the Dalabute fault is estimated by the present offset of the two mélange belts.

Figure 11: synoptic chart of the major episodes of magmatism, deformation and sedimentation that affected West Junggar during Carboniferous and Permian. The Carboniferous is marked by syn-accretion sedimentation, and is accompanied by a continuous deformation, and magmatism in the arc and fore-arc regions. The Late Carboniferous to Permian stage is characterized by moderate continental erosion, alkaline magmatism and transcurrent brittle deformation. Hachures in boxes correspond to periods where age assignment is uncertain.

Figure 12: tentative reconstruction of the Late Paleozoic evolution of West Junggar in the regional frame of Central Asia. The time-evolution in Kazakhstan and northwestern China is based on palaeomagnetic data (Van der Voo et al., 2008; Choulet et al., in press). Carboniferous closure of the Junggar Ocean by oroclinal bending lead to buckling of the active margin (1); subsequent relative rotation of a part of this margin give an oceanward concave shape of the margin and induced obliquity of the subduction zone. Ridge subduction may also be implicated in this process (2). Such a configuration may have favoured continuous deformation inside the upper plate and impeded large transcurrent displacements. In Late Carboniferous (305 Ma), oceanic domains have almost disappeared by subduction, and in response to the buckling of the margin, large transcurrent faults started to develop (3); this led to the destruction of the orocline and induced opposite relative rotations of West Junggar and North Kazakhstan ribbon margins (4). During the Permian (280 Ma), the counterclockwise rotation of West Junggar modified the geometry of the oblique convergent

zone that turned into a convex shape toward Junggar (5); it may favour the initiation of strike-slip faults and lateral displacement of units within West Junggar. The continuous transcurrent faulting throughout Central Asia (6) probably kept up this "Sunda style tectonics". KZK: Kazakhstan, NTS: North Tianshan, WJG: West Junggar. Faults abbreviations are the same as in figure 1b.

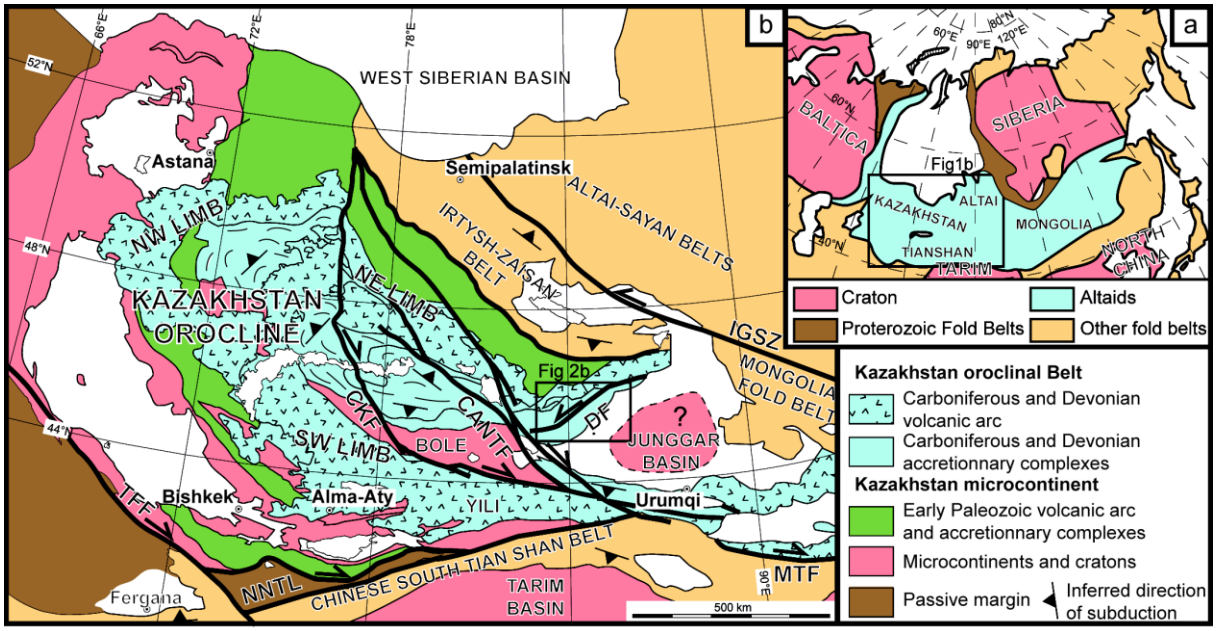
b
a
WEST SIBERIAN BASIN
Astana
Semipalatinsk
ALTAI-SAYAN BELTS
IRTYSH-ZAISAN BELT
NW LIMB
NE LIMB
KAZAKHSTAN OROCLINE
IGSZ
MONGOLIA FOLD BELT
Fig 2b
CKF
CANTF
DF
SW LIMB
BOLE
JUNGGAR BASIN
Bishkek
Alma-Aty
YILI
Urumqi
IFF
CHINESE SOUTH TIAN SHAN BELT
NNTL
Fergana
TARIM BASIN
MTF
500 km
BALTICA
SIBERIA
Fig1b
KAZAKHSTAN
ALTAI
MONGOLIA
TIANSHAN
TARIM
NORTH CHINA
Craton
Altaids
Proterozoic Fold Belts
Other fold belts
Kazakhstan oroclinal Belt
Carboniferous and Devonian volcanic arc
Carboniferous and Devonian accretionnary complexes
Kazakhstan microcontinent
Early Paleozoic volcanic arc and accretionnary complexes
Microcontinents and cratons
Passive margin
Inferred direction of subduction

Figure 1

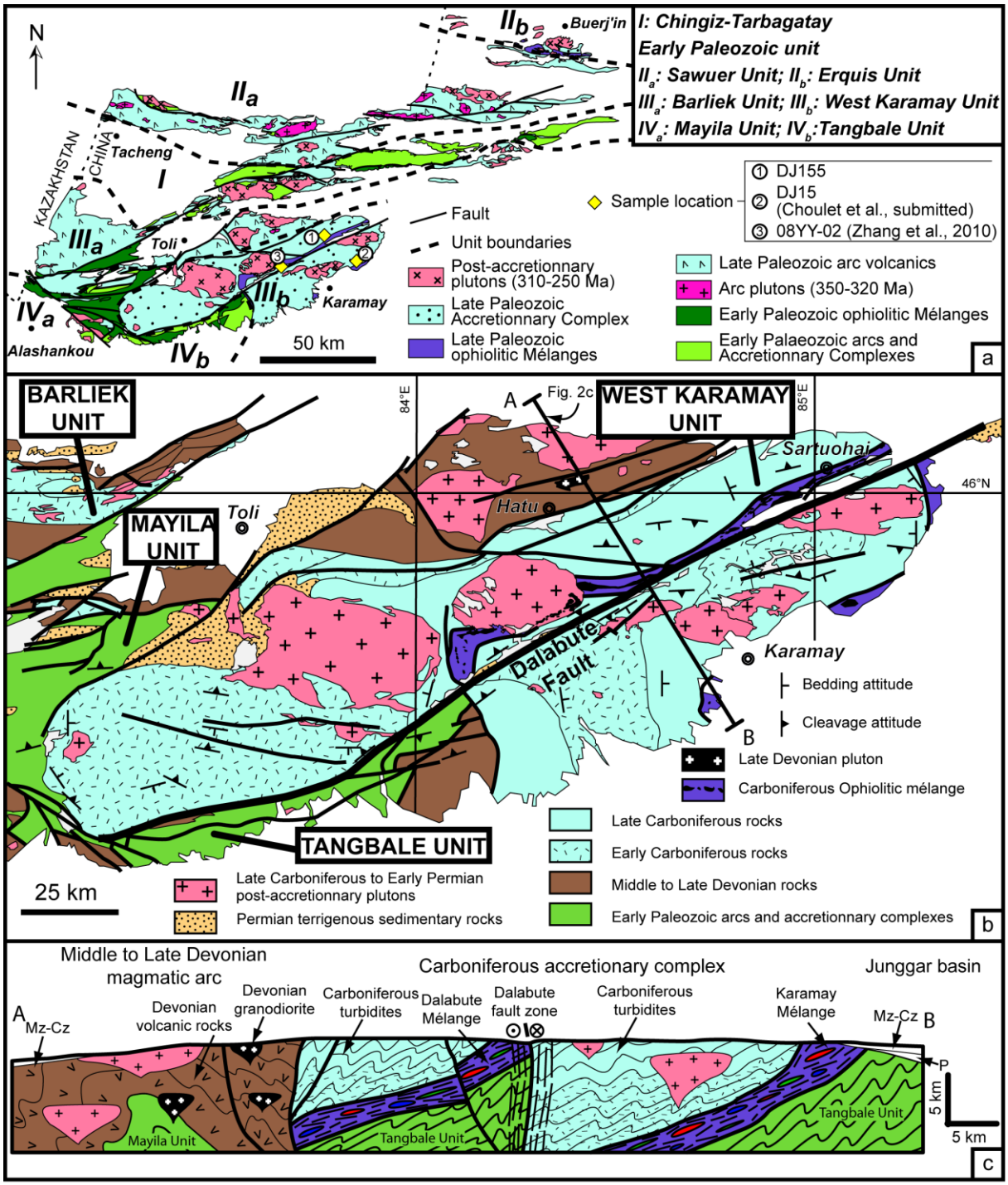
N
KAZAKHSTAN
CHINA
Tacheng
Buerj'in
Toli
Karamay
Alashankou
50 km
I: Chingiz-Tarbagatay
Early Paleozoic unit
II_a: Sawuer Unit; II_b: Erquis Unit
III_a: Barliek Unit; III_b: West Karamay Unit
IV_a: Mayila Unit; IV_b:Tangbale Unit
① DJ155
② DJ15 (Choulet et al., submitted)
③ 08YY-02 (Zhang et al., 2010)
Sample location
Fault
Unit boundaries
Post-accretionnary plutons (310-250 Ma)
Late Paleozoic Accretionnary Complex
Late Paleozoic ophiolitic Mélanges
Late Paleozoic arc volcanics
Arc plutons (350-320 Ma)
Early Paleozoic ophiolitic Mélanges
Early Palaeozoic arcs and Accretionnary Complexes
a
BARLIEK UNIT
MAYILA UNIT
TANGBALE UNIT
WEST KARAMAY UNIT
84°E
85°E
46°N
Fig. 2c
Sartuohai
Hatu
Dalabute Fault
Bedding attitude
Cleavage attitude
Late Devonian pluton
Carboniferous Ophiolitic mélange
Late Carboniferous rocks
Early Carboniferous rocks
Middle to Late Devonian rocks
Early Paleozoic arcs and accretionnary complexes
Late Carboniferous to Early Permian post-accretionnary plutons
Permian terrigenous sedimentary rocks
25 km
b
Middle to Late Devonian magmatic arc
Carboniferous accretionary complex
Junggar basin
Mz-Cz
Devonian volcanic rocks
Devonian granodiorite
Carboniferous turbidites
Dalabute Mélange
Dalabute fault zone
Carboniferous turbidites
Karamay Mélange
Mayila Unit
Tangbale Unit
Tangbale Unit
P
5 km
5 km
c

Figure 2

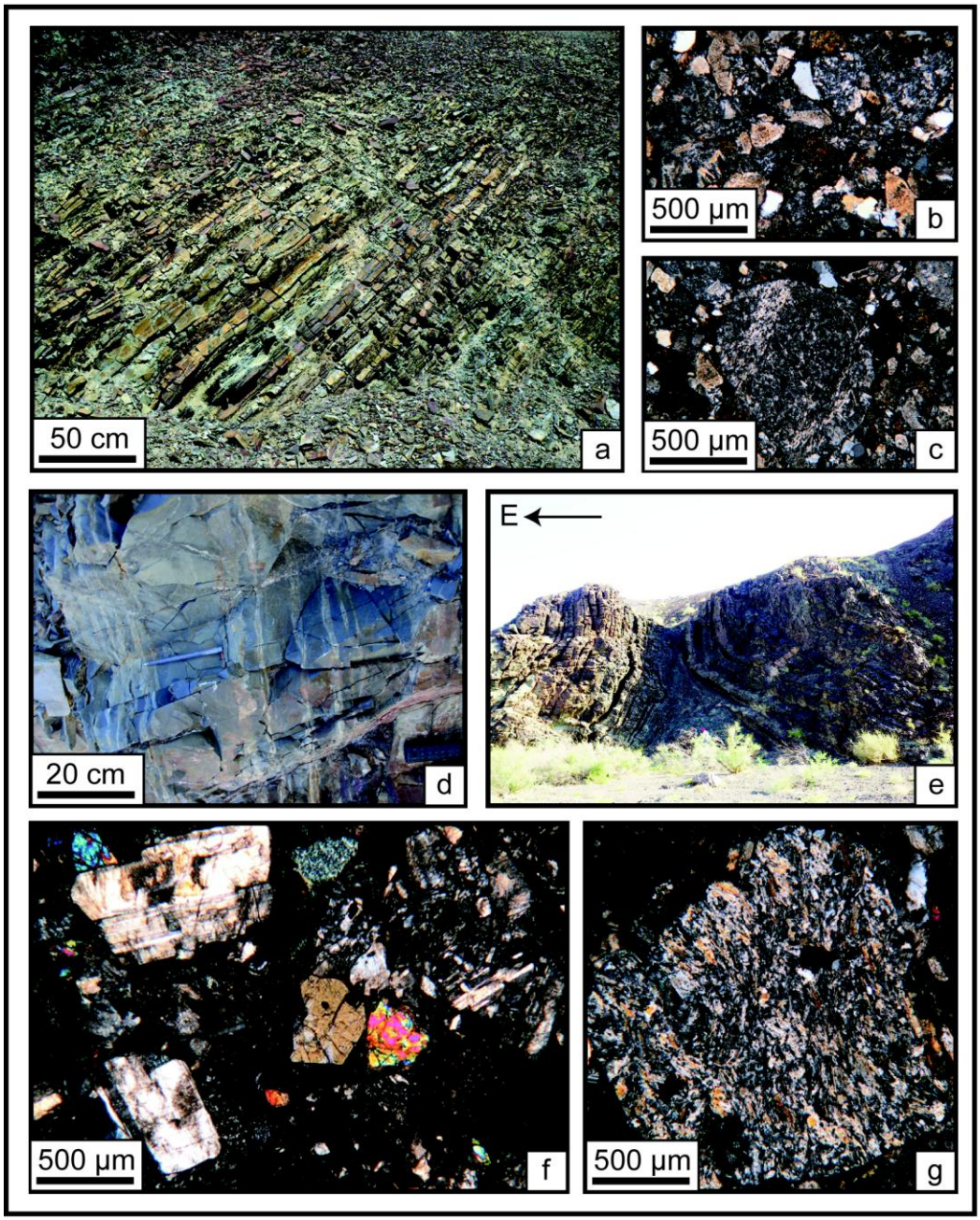

Figure 3

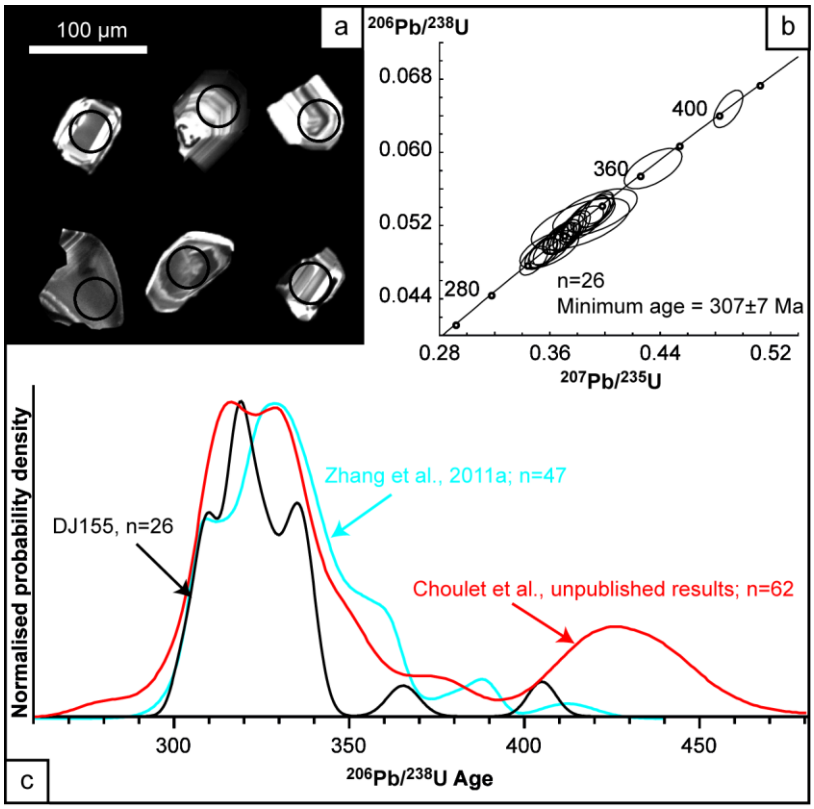
100 µm
a
b
$^{206}Pb/^{238}U$
0.068
0.060
0.052
0.044
400
360
280
n=26
Minimum age = 307±7 Ma
0.28
0.36
0.44
0.52
$^{207}Pb/^{235}U$
Normalised probability density
DJ155, n=26
Zhang et al., 2011a; n=47
Choulet et al., unpublished results; n=62
300
350
400
450
$^{206}Pb/^{238}U$ Age
c

Figure 4

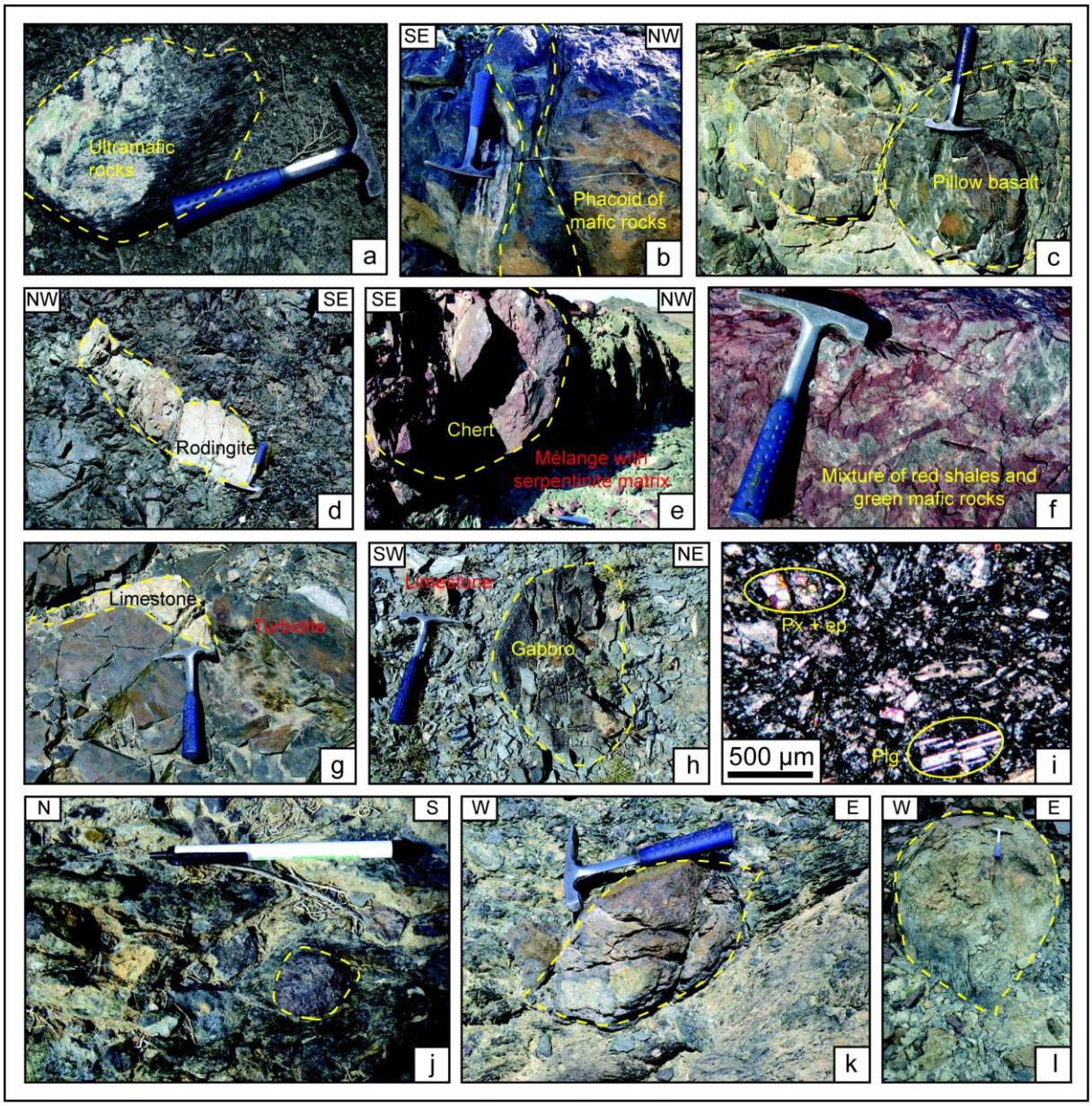
Ultramafic rocks
a
SE
NW
Phacoid of mafic rocks
b
Pillow basalt
c
NW
SE
Rodingite
d
SE
NW
Chert
Mélange with serpentinite matrix
e
Mixture of red shales and green mafic rocks
f
Limestone
Turbidite
g
SW
NE
Limestone
Gabbro
h
Px + ep
500 µm
Plg
i
N
S
j
W
E
k
W
E
l

Figure 5

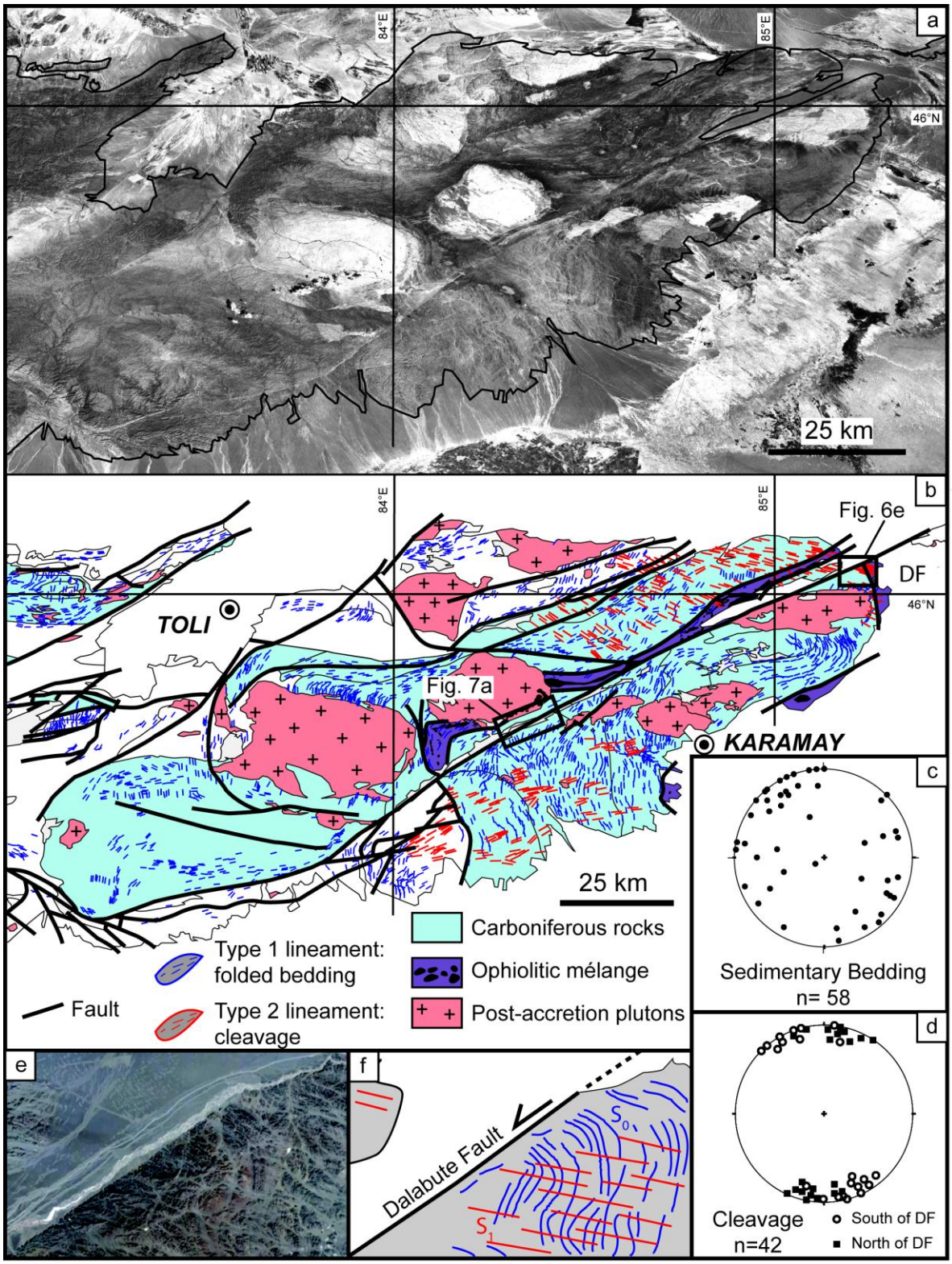
a
84°E
85°E
46°N
25 km
b
Fig. 6e
DF
TOLI
Fig. 7a
KARAMAY
25 km
Carboniferous rocks
Ophiolitic mélange
Post-accretion plutons
Type 1 lineament: folded bedding
Type 2 lineament: cleavage
Fault
c
Sedimentary Bedding
n= 58
d
Cleavage
n=42
South of DF
North of DF
e
f
Dalabute Fault
S_0
S_1

Figure 6

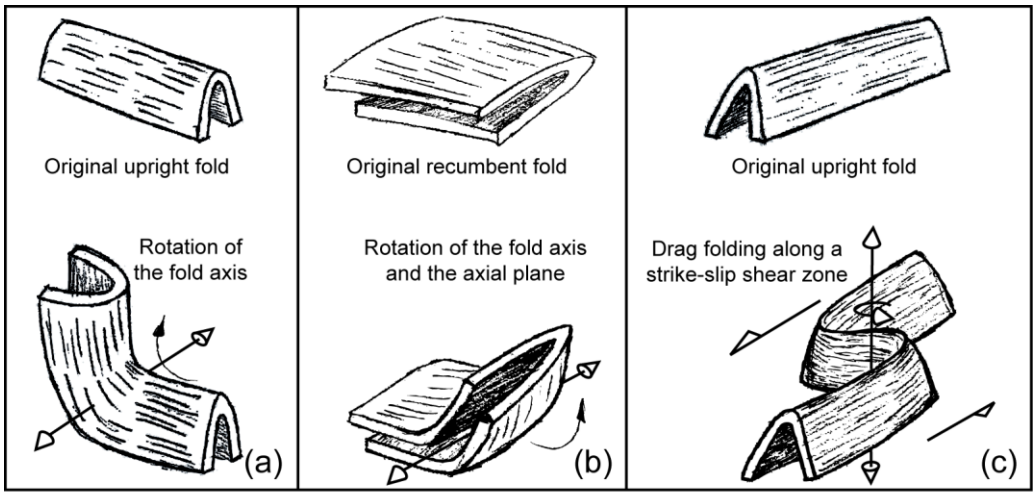
Original upright fold
Rotation of
the fold axis
(a)
Original recumbent fold
Rotation of the fold axis
and the axial plane
(b)
Original upright fold
Drag folding along a
strike-slip shear zone
(c)

Figure 7

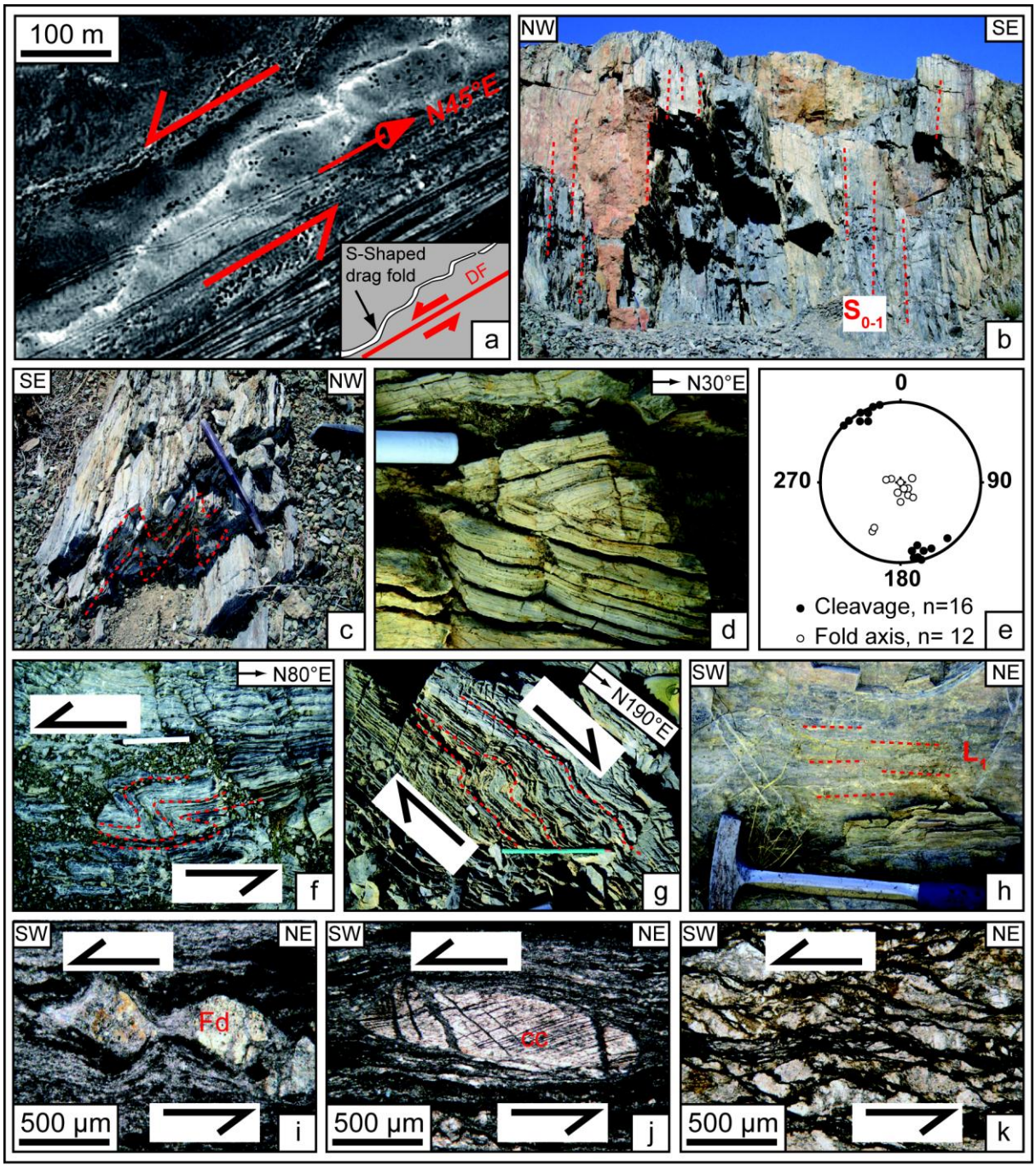
100 m
N45°E
S-Shaped
drag fold
DF
a
NW
SE
S_{0-1}
b
SE
NW
c
N30°E
d
0
270
90
180
Cleavage, n=16
Fold axis, n= 12
e
N80°E
f
N190°E
g
SW
NE
L_1
h
SW
NE
Fd
500 µm
i
SW
NE
cc
500 µm
j
SW
NE
500 µm
k

Figure 8

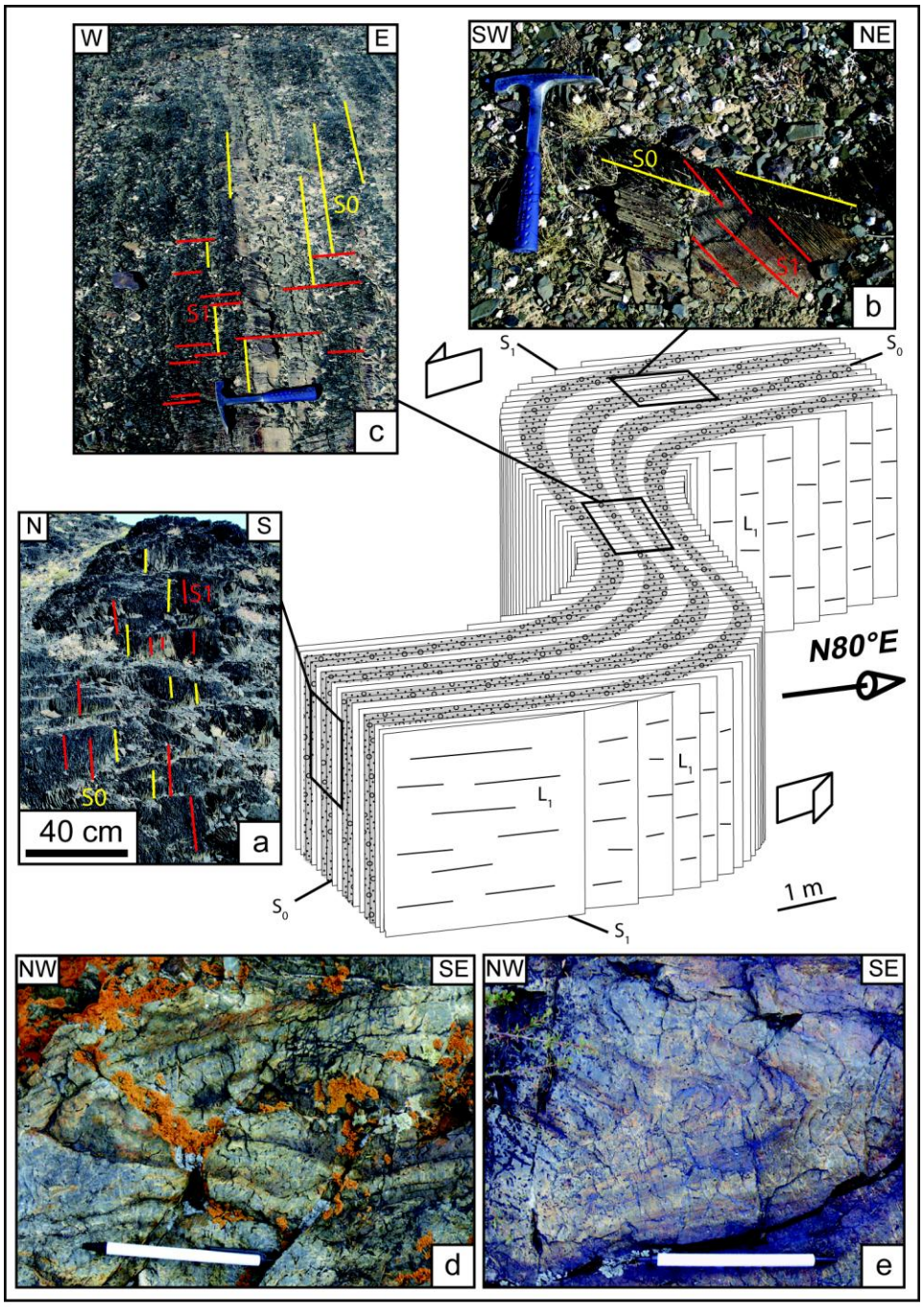
W
E
S0
S1
c
SW
NE
S0
S1
b
N
S
S1
S0
40 cm
a
S1
S0
L1
L1
L1
N80°E
1 m
S0
S1
NW
SE
d
NW
SE
e

Figure 9

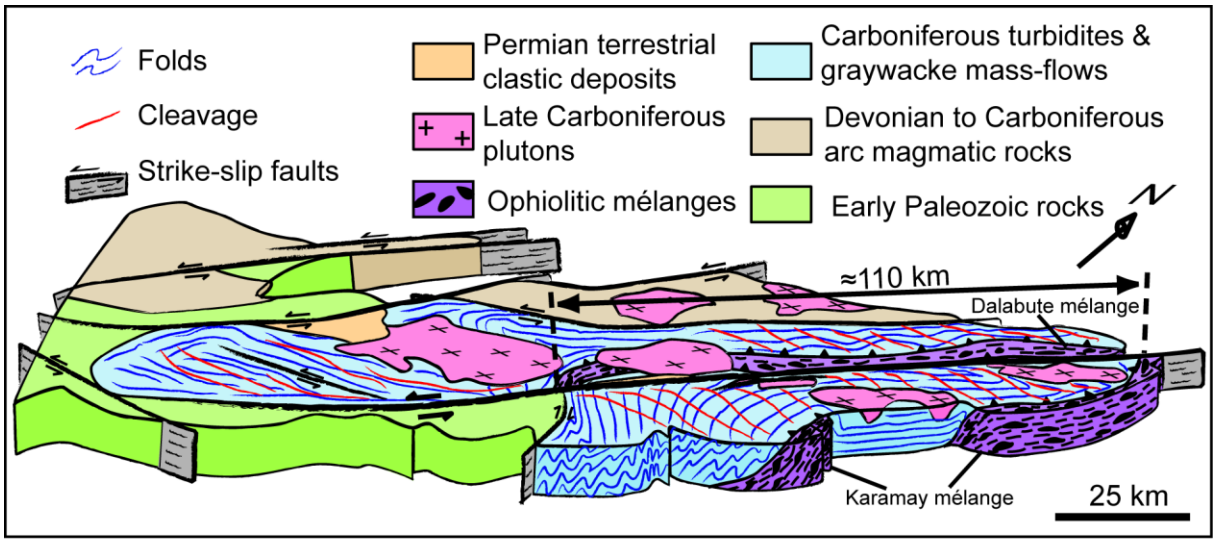
Folds
Cleavage
Strike-slip faults
Permian terrestrial clastic deposits
Late Carboniferous plutons
Ophiolitic mélanges
Carboniferous turbidites & graywacke mass-flows
Devonian to Carboniferous arc magmatic rocks
Early Paleozoic rocks
N
≈110 km
Dalabute mélange
Karamay mélange
25 km

Figure 10

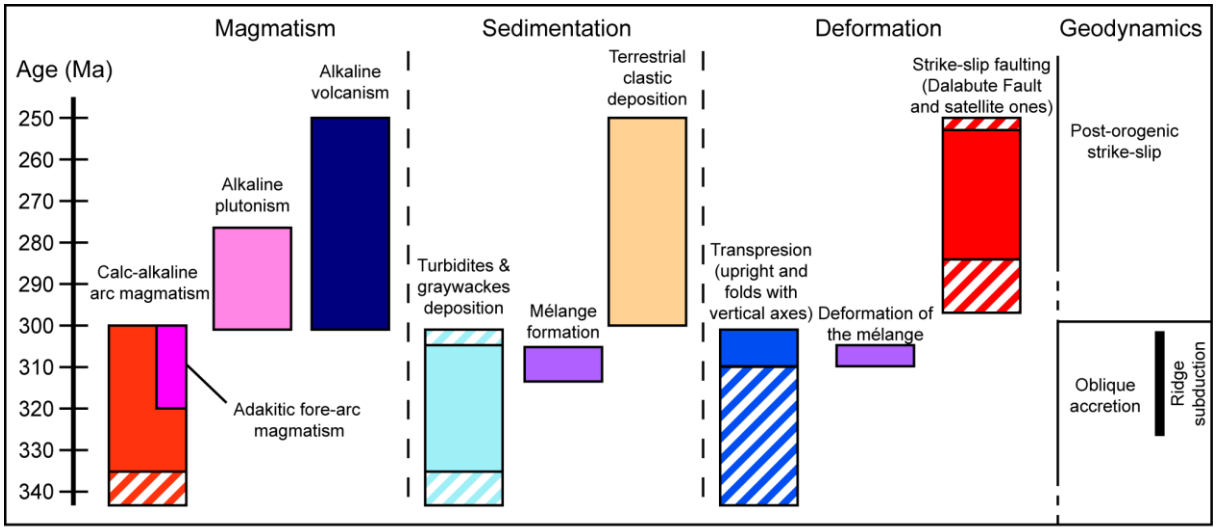
Magmatism
Sedimentation
Deformation
Geodynamics
Age (Ma)
250
260
270
280
290
300
310
320
330
340
Alkaline volcanism
Alkaline plutonism
Calc-alkaline arc magmatism
Adakitic fore-arc magmatism
Terrestrial clastic deposition
Turbidites & graywackes deposition
Mélange formation
Transpresion (upright and folds with vertical axes)
Deformation of the mélange
Strike-slip faulting (Dalabute Fault and satellite ones)
Post-orogenic strike-slip
Oblique accretion
Ridge subduction

Figure 11

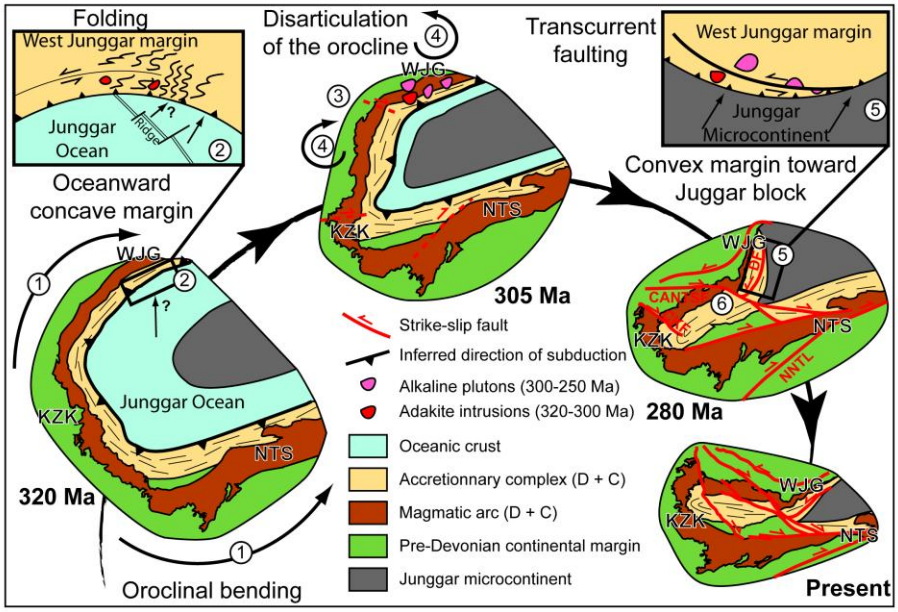
Folding
West Junggar margin
Junggar Ocean
Ridge
Oceanward concave margin
Disarticulation of the orocline
Transcurrent faulting
West Junggar margin
Junggar Microcontinent
Convex margin toward Juggar block
WJG
KZK
NTS
305 Ma
CANT
DF
NNTL
280 Ma
320 Ma
Junggar Ocean
Oroclinal bending
Present
Strike-slip fault
Inferred direction of subduction
Alkaline plutons (300-250 Ma)
Adakite intrusions (320-300 Ma)
Oceanic crust
Accretionnary complex (D + C)
Magmatic arc (D + C)
Pre-Devonian continental margin
Junggar microcontinent

Figure 12